

Phenomenology of the Higgs and Flavour Physics In the Standard Model and Beyond

DISSERTATION

zur Erlangung des akademischen Grades

doctor rerum naturalium
(Dr. rer. nat.)
im Fach Physik

eingereicht an der
Mathematisch-Wissenschaftlichen Fakultät
Humboldt-Universität zu Berlin

von

M.Sc. Lina Alasfar
geboren am 27.09. 1994 in Riad

Präsidentin der Humboldt-Universität zu Berlin:
Prof. Dr.-Ing. Dr. Sabine Kunst

Dekan der Mathematisch-Wissenschaftlichen Fakultät:
Prof. Dr. Elmar Kulke

Gutachter:

1. Prof. Dr. R. Gröber, Humboldt-Universität zu Berlin
2. Prof. Dr. Dr. M. Musterman, Potsdam-Institut für Klimafolgenforschung
3. Prof. Dr. M. Mustermann², Heidelberg

Tag der mündlichen Prüfung: 06. November 2013

Contents

I	Higgs Physics	1
1	The Standard Model Higgs boson	3
1.1	Spontaneous symmetry breaking	3
1.1.1	Nambu-Goldstone theorem	6
1.2	The Higgs mechanism	6
1.3	Yukawa interaction	9
1.4	The Higgs and EW precision observables	10
1.4.1	Custodial symmetry	12
2	Constraints on the Higgs properties	17
2.1	Theoretical constraints	17
3	Higgs and effective field theories	19
II	Single Higgs Processes at the LHC	21
4	Overview of Higgs production at colliders	23
5	Four top operator in Higgs production and decay	25
6	Associated Zh production via gluon fusion at NLO	27
6.1	Overview	27
6.2	Definitions	29
6.3	Expansion in the transverse momentum	31
6.4	LO Comparison	33
6.5	Renormalisation	35
6.5.1	Gluon wavefunction	37
6.5.2	Strong coupling constant	38
6.5.3	Top mass	38
6.5.4	Larin counter-term	38
6.5.5	All terms together	38
6.6	IR subtraction	39
6.7	Outline of the NLO Computation	39

6.8 Conclusion	40
III Higgs Pair at Hadron Colliders	43
7 Overview of Higgs pair production at colliders	45
8 Higgs pair as a probe for light Yukawas	49
9 Optimised search for Higgs pair via Interpretable machine learning	51
A Details of Zh calculation	53
A.1 Orthogonal Projectors in $gg \rightarrow ZH$	53
A.2 Two-loop Results	54

Part I

Higgs Physics

1 The Standard Model Higgs boson

It's very nice to be right sometimes...
it has certainly been a long wait.

Peter Higgs

1.1 Spontaneous symmetry breaking

Before talking about symmetry breaking, we need to discuss the concept of symmetry in physics. Symmetry has an essential role in studying physical systems. It manifests not only as a geometric feature of physical objects but also in the dynamics of physical systems. For example, one can find symmetries in the equation of motion, Lagrangians/Hamiltonians and actions. The magnetisation of materials is a good example of the role that symmetry plays in describing physical behaviour. For instance, **paramagnetic** materials have a positive magnetic susceptibility χ_B due to the random arrangement of their electrons' spins. The paramagnetic material spins arrangement will therefore possess rotational symmetry. The material has no *preferred direction* in space [1]. On the contrary, **ferromagnetic** materials with the electrons' spins aligned in a certain direction, will not have such symmetry as there will be a preferred direction, see Figure 1.1.

In particle physics and quantum field theory, symmetry plays an essential role in the taxonomy and dynamics of elementary particles and their bound states, i.e. hadrons, cf. [2, 3]. There are two types of symmetries considered when studying elementary particles and their quantum fields: external and internal symmetries. The first is the symmetry of the spacetime background. Typically, this is a four-dimensional Poincaré symmetry. However, in some models, higher spacetime dimensions or non-flat geometries are considered. Though there is no current evidence of higher dimensions or indications of non-flat spacetime from colliders and cosmological observations [4]. The second class of symmetries is internal symmetries stemming from the quantum nature of these particles/fields. Because their state is described by a **ray** in complex Hilbert/Fock spaces, internal symmetries are simply symmetries of rotations in these spaces that keep the action variation unchanged. Internal symmetries are usually described in terms of simple or product of simple **Lie groups**, e.g. $SU(N)$ ¹, and particles/fields will be arranged

¹Gauge theories based on finite groups have been investigated in the literature, but their phenomeno-

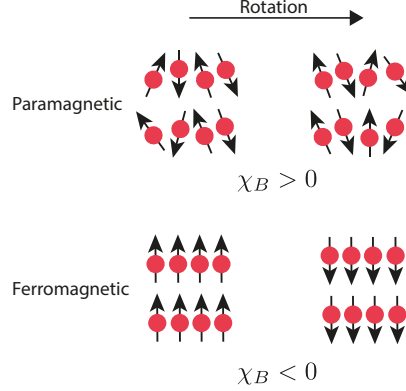


Figure 1.1. In paramagnetic materials, the spins are randomly distributed such that a rotation performed on the system will keep the spin distribution invariant. However, for ferromagnetic materials, where the spins are aligned in a single direction, the symmetry is broken, and the system has a preferred direction.

as multiplets in some representation of the groups. The rotations of the states could be parametrised by constants. In this case, the symmetry is called **global**, or fields of spacetime, where the symmetry is then called **local** or **gauged**.

Gauge symmetries describe rotations in the state space that depend on spacetime, the generator of the gauge transformations could propagate between two spacetime points. This is the way particle/field interactions are described in quantum field theory. The generators of these gauge transformations are called gauge bosons, and they mediate the interactions between the particles/fields and transform under the adjoint representation of the gauge group. Hence, we observe that gauge symmetries are the basis of describing the fundamental interactions of nature, which we call **gauge theories**.

An example of a gauge theory that is realised in nature is the **Standard Model** (SM). Which is a gauge theory based on the group $G_{\text{SM}} := SU(3)_C \otimes SU(2)_L \otimes U(1)_Y$. The first simple group is for the *strong* interaction described by quantum chromodynamics (QCD). The product of the two remaining groups $SU(2)_L \otimes U(1)_Y$ forms the Weinberg-Salam *electroweak* (EW) model [7, 8, 9], where $SU(2)_L$ describes the weak interaction which only couples to *left handed* fermions and $U(1)_Y$ is the weak hypercharge Y gauge group, defined by the formula

$$Y = 2(Q - T_3). \quad (1.1)$$

Where Q is the electric charge and T_3 is the third component of the weak isospin. A description of the matter content of the SM and their multiplicities with respect to G_{SM} is shown in [Table 1.1](#)

The SM has been very successful at describing particle interactions even when chal-

logical significance is yet to be further investigated [5, 6]

Particle/Field	G_{SM} multiplicity	mass [GeV]
$Q = \begin{pmatrix} u_L \\ d_L \end{pmatrix}, \begin{pmatrix} c_L \\ s_L \end{pmatrix}, \begin{pmatrix} t_L \\ b_L \end{pmatrix}$	$(\mathbf{3}, \mathbf{2}, 1/6)$	$m_u = 2.16 \cdot 10^{-3}, m_d = 2.67 \cdot 10^{-3}$
$U = u_R, s_R, t_R$	$(\mathbf{3}, \mathbf{1}, 2/3)$	$m_c = 0.93 \cdot 10^{-2}, m_s = 1.27$
$D = d_R, s_R, b_R$	$(\mathbf{3}, \mathbf{1}, -1/3)$	$m_t = 172.4, m_b = 4.18$
$L = \begin{pmatrix} \nu_{e,L} \\ e_L \end{pmatrix}, \begin{pmatrix} \nu_{\mu,L} \\ \mu_L \end{pmatrix}, \begin{pmatrix} \nu_{\tau,L} \\ \tau_L \end{pmatrix}$	$(\mathbf{1}, \mathbf{2}, -1/2)$	$m_e = 0.511 \cdot 10^{-3}, m_\mu = 1.05 \cdot 10^{-2}$
$E = e_R, \mu_R, \tau_R$	$(\mathbf{1}, \mathbf{1}, -1)$	$m_\tau = 1.77, m_\nu = ??$
$g/G_\mu^A, A = 1 \dots 8$	$(\mathbf{8}, \mathbf{1}, 0)$	0.0
γ/A_μ	$(\mathbf{1}, \mathbf{1}, 0)$	0.0
W_μ^\pm	$(\mathbf{1}, \mathbf{3}, 0)$	80.379
Z_μ	$(\mathbf{1}, \mathbf{3}, 0)$	91.1876
h	$(\mathbf{1}, \mathbf{2}, 1/2)$	125.10

Table 1.1. The SM constituents, their multiplicities with respect to the SM gauge group $G_{\text{SM}} := SU(3)_C \otimes SU(2)_L \otimes U(1)_Y$ and masses. The mass of the neutrinos ν is zero according to the SM prediction, but observations suggest that they are massive, and only the difference between the three masses is known [10]. The values of the masses are taken from the Particle Data Group (PDG) [4], and used throughout this thesis.

lenged by numerous precision tests at LEP and SLD [11, 12, 13, 14] and later at DØ [15] and the LHC [16, 17] Nevertheless, it fails to describe the ground state if only the fermion and gauge sectors are considered. The reason for this shortcoming is that the W^\pm and Z bosons have a mass, this violates the EW gauge symmetry. This can be easily seen by looking at the mass term of a spin 1 field B_μ^A

$$\mathcal{L} = m_B B^{A,\mu} B_\mu^A, \quad (1.2)$$

and performing an $SU(N)$ gauge transformation

$$B_\mu^A \rightarrow B_\mu^A + \partial_\mu \Lambda^A + g \varepsilon_{BC}^A B_\mu^B \Lambda^C. \quad (1.3)$$

We see that the mass term is invariant under these transformations. Secondly, because the SM is a chiral theory, as only left-handed fermions would be doublets under $SU(2)_L$, the Dirac mass term

$$\mathcal{L}_D = m_D \bar{\psi}_L \psi_R + \text{h.c.}, \quad (1.4)$$

cannot be a singlet under $SU(2)_L$, hence also violating the EW symmetry. Despite quark and lepton masses being forbidden by the EW symmetry, we indeed observe that they do have a mass, and since they also carry charges this mass has to be a Dirac mass.

In order for the EW model to be consistent at the ground state like it is in the interaction states. A mechanism for spontaneous symmetry breaking going from an

interaction state to the vacuum ought to be introduced.

1.1.1 Nambu-Goldstone theorem

Coming back to the example of the paramagnetic-ferromagnetic materials, when heated above a certain temperature, known as the **Curie Temperature** T_C will undergo a phase transition and become paramagnetic (losing their permanent magnet property), in the mean-field theory approximation the magnetic susceptibility is related to the temperature of the metal via the relation

$$\chi_B \sim (T - T_C)^{-\gamma}, \quad (1.5)$$

where γ is a critical exponent. We see that if the metal temperature $T > T_C$ the metal is in an *disordered phase* and when $T < T_C$ it is in the *ordered phase*, i.e. χ_B is the **order parameter** of this system. At the Curie temperature, the system will be at the *critical point* where the susceptibility is divergent. The exponent γ is not used to describe the system at the critical point. There is a “pictorial” description of the metal at the critical point which is helpful in picturing the Goldstone theorem. Starting at $T > T_C$, the metal would be in a paramagnetic phase, where the spins are randomly arranged. As the temperature becomes lower and lower, thermal fluctuations start to lessen. One or more regions of the metal, some of the spins will start to get aligned. With continued cooling, nearing T_C , these turned spins will affect their neighbours turning them into their directions. At the critical point $T = T_C$, the system behaves in a peculiar manner, when one would see regions of spins in “up” and others in “down” directions. The system will resemble a fractal of these regions, becoming scale-invariant. Additionally, waves of oscillating local magnetisation will propagate. These waves, or spinless quasiparticles (called **Magnons**) are Goldstone bosons emerging from spontaneous symmetry breaking. Which will manifest at $T < T_C$ as the spins will be arranged in a certain single direction and the metal becomes ferromagnetic.

Theorem 1 (Nambu-Goldstone). When a continuous symmetry has a conserved currents but broken in the ground state (vacuum) is called to be spontaneously broken. There is a scalar boson associated with each broken generator of this spontaneously broken symmetry. The modes of these bosons are fluctuations of the order parameter.

This theorem first emerged from condensed matter physics, particularly superconductors [18, 19]. However, it soon got applied to relativistic quantum field theories [20].

1.2 The Higgs mechanism

In order to solve the aforementioned shortcomings of the Weinberg-Salam model, Nambu-Goldstone theorem has been first proposed by P. W. Anderson [21]. However, the way

that Anderson formulated his theory was unfamiliar to particle physicists and used a non-relativistic picture to illustrate how photons could gain mass in an electron plasma with a plasma frequency ω_p

$$m_\gamma^{\text{plasma}} = \frac{\hbar\omega_p}{c^2} \quad (1.6)$$

Later on, a theory that explains the mass generation of the EW gauge bosons has been published in an almost simultaneous manner by R. Braut and F. Englert [22], P. Higgs [23] and G. Guralnik, C. R. Hagen, and T. Kibble [24, 25]². The Higgs mechanism starts by considering the spontaneous symmetry breaking (SSB) of the EW sector of the SM via the pattern

$$SU(2)_L \otimes U(1)_Y \longrightarrow U(1)_Q \quad (1.7)$$

This is achieved by the vacuum expectation value (vev) of a complex scalar field $\phi \sim (\mathbf{1}, \mathbf{2}, +1/2)$, with the Lagrangian

$$\mathcal{L} = D_\mu \phi^* D^\mu \phi - V, \quad V := \mu^2 \phi^* \phi + \lambda(\phi^* \phi)^2, \quad (1.8)$$

where ϕ is given explicitly by

$$\phi = \begin{pmatrix} \phi^1 + i\phi^2 \\ \frac{1}{\sqrt{2}}(h + v) - i\phi^3 \end{pmatrix} \quad (1.9)$$

The covariant derivative

$$D_\mu = \partial_\mu - ig_2 \frac{\sigma_a}{2} W_\mu^a - ig_1 \frac{1}{2} B_\mu, \quad (1.10)$$

dictates the coupling between the Higgs field and the EW gauge bosons and g_3 , g_2 and g_1 are, respectively, the coupling constants of $SU(3)_C$, $SU(2)_L$ and $U(1)_Y$. The minimum of the scalar potential is then obtained by

$$\frac{\partial V}{\partial \phi} \Big|_{\phi \rightarrow v} = 0, \quad (1.11)$$

which for a tachyonic mass $\mu^2 < 0$ will have a real non-vanishing values v corresponding to the vev of this field $\langle \phi \rangle = \begin{pmatrix} 0 \\ \frac{v}{\sqrt{2}} \end{pmatrix}$.

According to Nambu-Goldstone theorem, the three broken generators of $SU(2)_L \otimes U(1)_Y$ will become massive, and they are the W^\pm and Z bosons, while the photon will remain massless. We will have three massless Goldstone bosons $G^\pm = \frac{1}{2}(\phi^1 \pm i\phi^2)$ and $G^0 =$

²All of these authors have contributed to the theory of SM spontaneous symmetry breaking (SSB). By calling it the ‘‘Higgs’’ mechanism or boson. I, by no means, have intended to ignore the role played by the rest, rather, I wanted to stick the most widely-used terminology in the field.

ϕ^3 that are “eaten” by the aforementioned massive photons. Where they become the longitudinal polarisations of W^\pm and Z boson. In order to see this more concretely, we start by looking at the terms of the EW Lagrangian where the field ϕ couples to the gauge bosons, in the unbroken phase

$$D_\mu \phi^* D^\mu \phi = \frac{1}{2} |\partial_\mu \phi|^2 + \frac{1}{8} g_2^2 |\phi|^2 |W_\mu^1 + iW_\mu^2|^2 + \frac{1}{8} |\phi|^2 |g_2 W_\mu^3 - g_1 B_\mu|^2 \quad (1.12)$$

After SSB, we write the gauge bosons in the mass basis

$$\begin{aligned} W_\mu^\pm &= \frac{1}{\sqrt{2}} (W_\mu^1 \pm iW_\mu^2), \\ Z_\mu &= \frac{1}{\sqrt{g_1^2 + g_2^2}} (g_2 W_\mu^3 - g_1 B_\mu), \\ A_\mu &= \frac{1}{\sqrt{g_1^2 + g_2^2}} (g_2 W_\mu^3 + g_1 B_\mu). \end{aligned} \quad (1.13)$$

From this, the electric charge is identified as the coupling constant to the photon A_μ

$$e = \frac{g_1}{\sqrt{g_1^2 + g_2^2}}. \quad (1.14)$$

It is useful to define **Weinberg angle** θ_W , an important EW parameter relating the electric charge to the weak coupling g_2

$$\sin \theta_W = \frac{e}{g_2} \approx 0.231214, \quad (1.15)$$

typically the sin and cos of the Weinberg angle are denoted by s_W and c_W , respectively. We use the unitary gauge, to absorb the Goldstone bosons into the W^\pm and Z longitudinal polarisations. In this gauge the Higgs doublet can be written as

$$\phi \rightarrow \begin{pmatrix} 0 \\ \frac{1}{\sqrt{2}}(h + v) \end{pmatrix}, \quad v = 246 \text{ GeV}. \quad (1.16)$$

With these substitutions, one can read off the masses of the gauge bosons their bilinear terms in (1.12)

$$m_W = \frac{vg_2}{2} \quad m_Z = \frac{v}{2} \sqrt{g_1^2 + g_2^2} \quad m_A = 0. \quad (1.17)$$

Since ϕ is a complex doublet. We have seen that it has four components, and three of them correspond to the Goldstone bosons, thus one remains physical h which is what

we now identify with the ‘‘Higgs boson’’ discovered in the Summer of 2012 [26, 27]. The couplings between the Higgs and the electroweak bosons is related to their mass via the vev

$$g_{hVV} = \frac{2m_V^2}{v}, \quad g_{hhVV} = \frac{2m_V^2}{v^2}. \quad (1.18)$$

By substituting (1.16), into the Higgs potential (1.8) one can write the mass of the physical Higgs boson in terms of the vev

$$m_h = \sqrt{2\lambda}v. \quad (1.19)$$

The physical Higgs mass is related to the μ parameter via the relation

$$m_h^2 = -2\mu^2, \quad (1.20)$$

One can see that the mass term after SSB changes its sign, characterising the order-parameter for this system, analogous to the magnetic susceptibility for the magnetisation of materials example. One could also identify the self-couplings of h , the trilinear and quartic couplings

$$g_{hhh} = 3\lambda v = 3\frac{m_h^2}{v}, \quad g_{hhhh} = 3\lambda = 3\frac{m_h^2}{v^2}. \quad (1.21)$$

1.3 Yukawa interaction

It is possible to also use the Higgs vev to give fermions their masses by introducing a Yukawa-interaction terms, first introduced by S. Weinberg [9]

$$\mathcal{L}_{\text{Yuk}} = -y_e \bar{L} \phi E - y_d \bar{Q} \phi D - y_u \bar{Q} \tilde{\phi} U + \text{h.c.}, \quad (1.22)$$

with $\tilde{\phi} = i\sigma_2 \phi$ and y_e, y_d, y_u are 3×3 matrices. These matrices are free parameters in the SM. As the Higgs boson acquires a the vev, the fermions will acquire a mass $m_f = v y'_f$ and the Higgs boson coupling to the fermions is given by

$$g_{h\bar{f}f} = \frac{m_f}{v}, \quad (1.23)$$

and the Yukawa matrices will be fixed in the mass basis y'_f by measurements of the fermion masses.

Leptonic Yukawa matrix is diagonal, with a degeneracy between the flavour and masses basis, this manifests as lepton family number conservation (the lepton family operator commutes with the Hamiltonian.). However, for the quarks, the situation is more complicated. One can rotate these matrices to the mass basis via a bi-unitary transformation

via the unitary matrices $\mathcal{V}_Q, \mathcal{U}_Q$ for $q = u, d$

$$y_q \longrightarrow y'_f = \mathcal{V}_q^\dagger y_q \mathcal{U}_q = \text{diag}(m_{q_1}, m_{q_2}, m_{q_3}). \quad (1.24)$$

However, there is no degeneracy here as the Hamiltonian does not commute with the quark flavour operator. This is because the transformation matrices for the up and down-type quarks are not the same. The charged EW quark currents contain flavour mixing described by the Cabibbo-Kobayashi-Maskawa (CKM) matrix [28, 29]. More details on the flavour sector of the SM are discussed in [Update the section](#). [Figure 1.2](#) shows all the SM couplings' strengths, with the thickness of the chord is proportional to the strength of the coupling, one can see the Higgs couplings in orange.

1.4 The Higgs and EW precision observables

Higgs physics is intertwined with the EW sector for example, the Higgs vev is determined from Fermi's constant $v = (\sqrt{2}G_F)^{-1/2}$, and is fixed by muon lifetime measurements, and comparing it with the theoretical predictions [30, 31, 32, 33]

$$\tau_\mu^{-1} = \frac{G_F^2 m_\mu^5}{192\pi^3} \left(1 - \frac{8m_e^2}{m_\mu^2}\right) \left[1 - 1.810 \frac{\alpha}{\pi} + (6.701 \pm 0.002) \left(\frac{\alpha}{\pi}\right)^2\right], \quad (1.25)$$

which leads to the numerical value of G_F [4]

$$G_F = 1.1663787(6) \cdot 10^{-5} \text{GeV}^{-2}, \quad (1.26)$$

given the value of the fine structure constant $\alpha^{-1} = 137.03599976(50)$.

Another important EW precision observable (EWPO) is the ratio between the W and Z masses

$$\rho = \frac{m_W^2}{c_W^2 m_Z^2}. \quad (1.27)$$

At leading order, this parameter is equal to unity in the SM. The ρ parameter depends on the representation of the scalar sector of the EW model having ϕ_i scalars with T_i weak isospin and $T_{3,i}$ being its third component, and a vev v_i , via the relation [34, 35]

$$\rho = \frac{\sum_i [T_i(T_i + 1) - T_{3,i}^2] v_i^2}{2 \sum_i T_{3,i}^2 v_i^2}. \quad (1.28)$$

From (1.28) one can see that a real triplet scalar, for instance, would not fit the experimental EW measurement of ρ . Hence, a complex doublet is the simplest scalar possible for the EW symmetry breaking, and the Higgs boson was expected to be seen almost four decades before its discovery. However, radiative corrections to the EW gauge

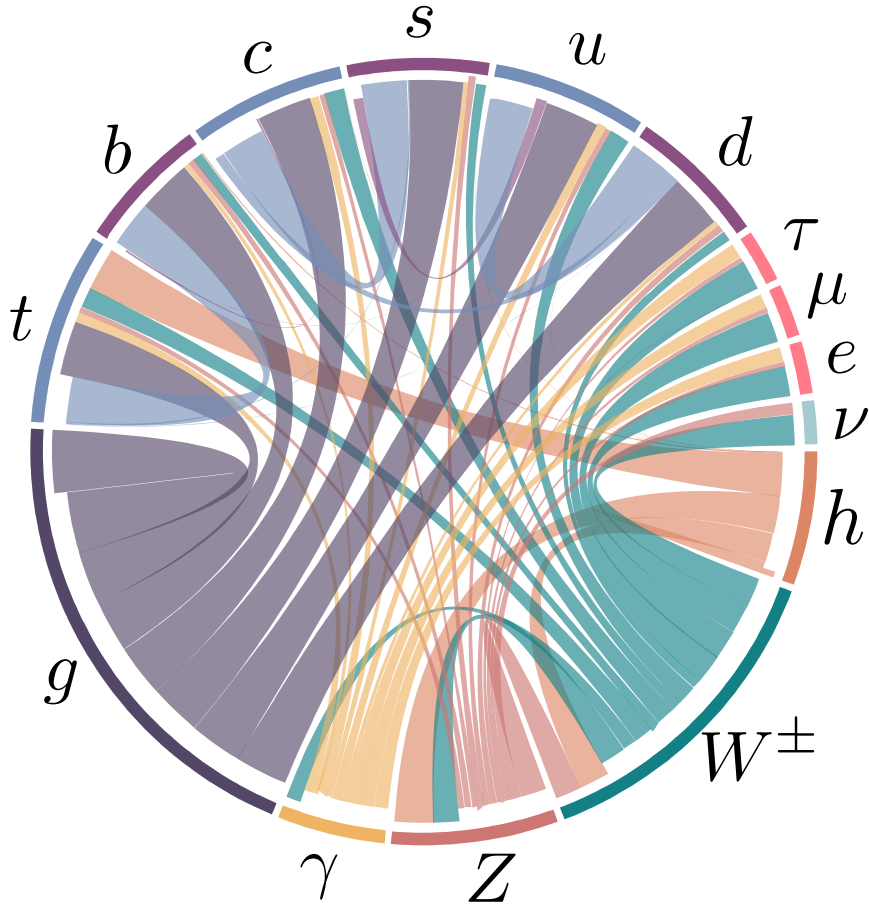


Figure 1.2. A chord diagram showing the SM couplings, with the coupling strength illustrated by the chord thickness. Higgs couplings are coloured in orange.

bosons mass from vacuum polarisation diagrams could potentially cause ρ to deviate significantly from unity. This is not the case, as the experimentally measured value of ρ [4]

$$\rho_{\text{exp}} = 1.00038 \pm 0.00020 \quad (1.29)$$

Additionally, it is possible to think of an extended Higgs sector, where there are multiple scalars with different $SU(2)_L$ multiplicities. Or, a composite Higgs sector, where the Higgs boson is a pseudo Nambu-Goldstone boson, cf. [36, 37]. How can such models be built assuring the ρ parameter is protected from change? The answer to this question lies in a symmetry of the Higgs Lagrangian known as custodial symmetry.

1.4.1 Custodial symmetry

After SSB, a residual global symmetry known as the custodial symmetry protects the ρ parameter from obtaining large radiative corrections at higher orders in perturbation theory. This symmetry must be kept in extended or composite Higgs models. This symmetry can be seen by rewriting the Higgs potential as

$$V = \frac{\lambda}{4} \left(\phi_1^2 + \phi_2^2 + \phi_3^2 + \phi_4^2 - 2\mu^2 \right)^2. \quad (1.30)$$

This potential is invariant under $SO(4) \simeq SU(2)_L \otimes SU(2)_R$ rotations. However, when the Higgs field acquires a non-vanishing vev, $\phi_4 \rightarrow h + v$, the potential becomes

$$V = \frac{\lambda}{4} \left(\phi_1^2 + \phi_2^2 + \phi_3^2 + h^2 + 2vh + v^2 - 2\mu^2 \right)^2, \quad (1.31)$$

which is only invariant under $SO(3) \simeq SU(2)_V$ transformations, the diagonal part of the original group. This global SSB pattern comes alongside the EW SSB of the gauge group $SU(2)_L \otimes U(1)_Y$ as global $SU(2)_L$ is itself the gauged $SU(2)_L$ group. Additionally the T^3 component of the $SU(2)_R$ global group is the gauged $U(1)_Y$ and the T^3 component of the custodial group $SU(2)_V$ is gauged as well and identified to be the electric charge operator, i.e. the generator of $U(1)_Q$.

$$\underbrace{SU(2)_R}_{\supset U(1)_Y} \otimes \overbrace{SU(2)_L}^{\text{gauged}} \longrightarrow \underbrace{SU(2)_V}_{\supset U(1)_Q}. \quad (1.32)$$

This pattern indicates that the symmetry is already broken by the gauging of the diagonal part of $SU(2)_R$ (the hypercharge). The custodial symmetry is only *approximate* in the limit of $g_1 \rightarrow 0$, and $\rho = 1$ is a consequence of $g_1 \neq 0$. The symmetry breaking pattern $\mathbf{2} \otimes \mathbf{2} = \mathbf{3} \oplus \mathbf{1}$ also allows us to identify the Goldstone bosons as the custodial triplet and the physical Higgs h as the custodial singlet, explaining the electric charge

pattern they have.

We could use the isomorphism between the special orthogonal and special unitary groups to parametrise the Higgs doublet as an $SU(2)_L \otimes SU(2)_R$ bidoublet

$$\mathcal{H} = (\tilde{\phi} \ \phi) = \frac{1}{\sqrt{2}} \begin{pmatrix} \phi_4 - i\phi_3 & \phi_1 + i\phi_2 \\ \phi_1 - i\phi_2 & \phi_4 + i\phi_3 \end{pmatrix}, \quad (1.33)$$

with the bi-unitary transformations

$$\mathcal{H} \longrightarrow \mathcal{U}_L \mathcal{H} \mathcal{U}_R^\dagger \quad (1.34)$$

which leaves any traces of the form $\text{Tr}(\mathcal{H}^\dagger \mathcal{H})$, invariant. The Higgs potential could be rewritten in terms of the bidoublet

$$V = -\frac{\mu^2}{2} \text{Tr}(\mathcal{H}^\dagger \mathcal{H}) + \frac{\lambda}{4} \left(\text{Tr}(\mathcal{H}^\dagger \mathcal{H}) \right)^2 \quad (1.35)$$

The vev is hence written in this representation as

$$\langle \mathcal{H} \rangle = \frac{v}{\sqrt{2}} \mathbb{1}_{2 \times 2}. \quad (1.36)$$

We can also look at the Yukawa sector, and observe that in the case where $y_u = y_d = y$, we can also write the left-handed and right-handed quarks as $SU(2)_L \otimes SU(2)_R$ bidoublets and $SU(2)_R$ doublets, respectively. Hence, the quark part of the Yukawa Lagrangian in (1.22) becomes

$$\mathcal{L}_{yuk} \supset \frac{y}{\sqrt{2}} (\bar{u}_L \ \bar{d}_L) \begin{pmatrix} \phi_4 - i\phi_3 & \phi_1 + i\phi_2 \\ \phi_1 - i\phi_2 & \phi_4 + i\phi_3 \end{pmatrix} \begin{pmatrix} u_R \\ d_R \end{pmatrix}, \quad (1.37)$$

which is invariant under custodial transformations, but when $y_u \neq y_d$, this Lagrangian term breaks custodial symmetry. Thus, the differences between the up-type and down-type quark masses $m_u - m_d$ are considered **spurions** of the custodial symmetry and one expects to see radiative corrections to ρ being proportional to these spurions.

In order to see this more concretely, we start by examining the radiative corrections that could contribute to the deviation of ρ from unity, i.e. $\Delta\rho$ these corrections are known as the **oblique correction**. These oblique corrections come from electroweak vacuum polarisations $\Pi_{VV}(p^2)$, as shown in Figure 1.3, for more details on these corrections and their calculation see Refs.. [38, 39]

The 1-loop correction to the ρ parameter is given in terms of the Π_{VV} by

$$\Delta\rho = \frac{\Pi_{WW}(0)}{m_W^2} - \frac{\Pi_{ZZ}(0)}{m_Z^2} \quad (1.38)$$

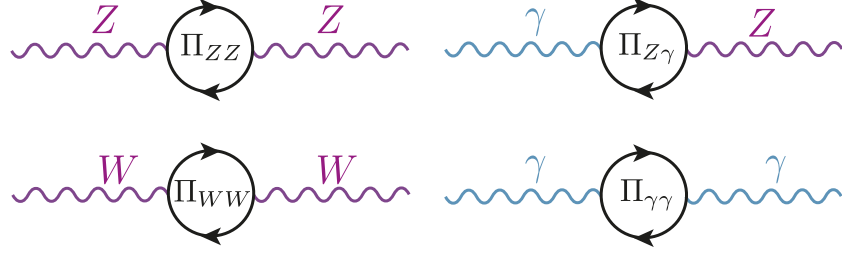


Figure 1.3. The oblique corrections, are radiative correction with electroweak gauge bosons propagators. Namely vacuum polarisations of the Z , W^\pm and γ bosons.

Where the dominant contributions are given by [40]

$$\Delta\rho = \frac{3G_F}{8\sqrt{2}\pi^2} \left((m_t^2 + m_b^2) - \frac{2m_t^2 m_b^2}{m_t^2 - m_b^2} \ln \frac{m_t^2}{m_b^2} \right) + \dots \quad (1.39)$$

Since $m_b \ll m_t$, the correction is non-vanishing, and (1.39) shows clearly how the radiative corrections are proportional to the spurions of the custodial symmetry. However, this radiative correction is absorbed into the SM definition of ρ , i.e. the $\overline{\text{MS}}$ definition of the ρ -parameter $\rho^{\overline{\text{MS}}}$.

One can study new physics (NP) effects that violates custodial symmetry, by looking at deviations from $\rho = 1$ from it. Given the experimentally measured value of ρ (1.29) many NP models violating custodial symmetry can already be excluded. Nevertheless, ρ alone does not capture the full story of EWPO's. For instance, adding a new quark doublet would not necessarily violate the custodial symmetry though it still can be excluded by EWPO. It is hence useful to introduce new parameters known as **Peskin-Takeuchi parameters** [41, 42, 39]

$$\begin{aligned} S &:= \frac{4c_W^2 s_W^2}{\alpha} \left[\frac{\Pi_{ZZ}^{\text{NP}}(m_Z^2) - \Pi_{ZZ}^{\text{NP}}(0)}{m_Z^2} - \frac{c_W^2 - s_W^2}{c_W s_W} \frac{\Pi_{Z\gamma}^{\text{NP}}(m_Z^2)}{m_Z^2} - \frac{\Pi_{\gamma\gamma}^{\text{NP}}(m_Z^2)}{m_Z^2} \right], \\ T &:= \frac{\rho^{\overline{\text{MS}}} - 1}{\alpha} = \frac{1}{\alpha} \left[\frac{\Pi_{WW}^{\text{NP}}(0)}{m_W^2} - \frac{\Pi_{ZZ}^{\text{NP}}(0)}{m_Z^2} \right], \\ U &:= \frac{4s_W^2}{\alpha} \left[\frac{\Pi_{WW}^{\text{NP}}(m_W^2) - \Pi_{WW}^{\text{NP}}(0)}{m_W^2} - \frac{c_W}{s_W} \frac{\Pi_{Z\gamma}^{\text{NP}}(m_Z^2)}{m_Z^2} - \frac{\Pi_{\gamma\gamma}^{\text{NP}}(m_Z^2)}{m_Z^2} \right] - S. \end{aligned} \quad (1.40)$$

The NP contributions to the EW vacuum polarisations $\Pi_{VV}^{\text{NP}}(p^2)$ could either come from loop or tree-level effects. Typically both T and U are related to custodial symmetry violation. However, U has an extra suppression factor of m_{NP}^2/m_Z^2 compared to T and

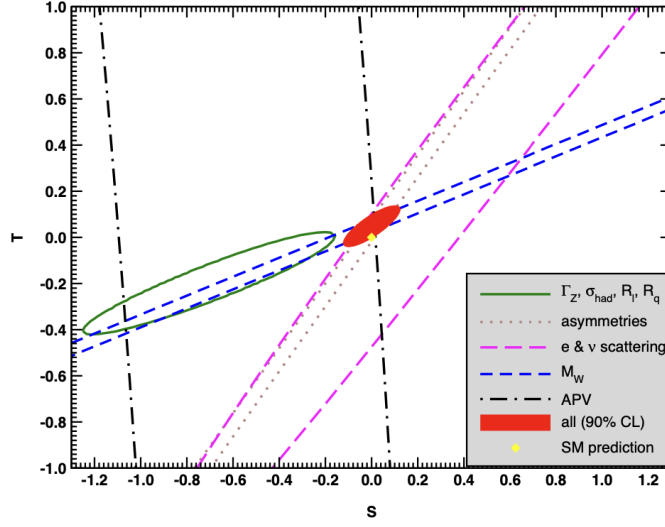


Figure 1.4. Fit results from various EWPO's for T and S setting $U = 0$. The contours show 1σ contours (39.35% for closed contours and 68% for the rest). This plot is obtained from the PDG [4]

S . The most recent fit result for these parameters is [4]

$$\begin{aligned} S &= -0.01 \pm 0.10, \\ T &= 0.03 \pm 0.13, \\ U &:= 0.02 \pm 0.11. \end{aligned} \tag{1.41}$$

But since T and S tend to give stronger constraint on NP, due to the suppression factor of U . One can perform a two-parameter fit of S and T setting $U = 0$, that shown in Figure 1.4, with the numerical values [4],

$$\begin{aligned} S &= 0.00 \pm 0.07, \\ T &= 0.05 \pm 0.06. \end{aligned} \tag{1.42}$$

The Peskin-Takeuchi parameters are important in constraining effective operators in the Higgs sector, namely

$$\begin{aligned} \hat{O}_S &= \phi^\dagger \sigma_i \phi W_{\mu\nu}^i B^{\mu\nu}, \\ \hat{O}_T &= |\phi^\dagger D_\mu \phi|^2. \end{aligned} \tag{1.43}$$

For example, \hat{O}_S appears in Technicolour models causing large deviations of S compared to its measured value [43, 44, 45, 41]. Moreover, The constraints on T parameter is

important for top mass generation as well as modifications to $Zb\bar{b}$ coupling in such models [46, 47]. We will revisit the \hat{O}_T when we discuss the Higgs and effective field theories in section [update here](#).

2 Constraints on the Higgs properties

In this chapter, the bounds on the Higgs sector will be discussed. Starting from an overview of the theoretical constraints on the Higgs potential, like the quantum triviality and unitarity. Then, the state-of-the-art experimental results on Higgs properties and couplings measurements will be discussed. However, despite many of the Higgs boson properties have been measured with good accuracy, there are still difficult observables in the Higgs sector and some open problems. These will be addressed at the end of this chapter.

2.1 Theoretical constraints

3 Higgs and effective field theories

Part II

Single Higgs Processes at the LHC

4 Overview of Higgs production at colliders

5 Four top operator in Higgs production and decay

6 Associated Zh production via gluon fusion at NLO

6.1 Overview

As we have seen in the previous sections, Higgs couplings to the weak vector bosons, i.e. Z and W is approaching the precision level. Moreover, the associated Higgs production with these bosons is the first channel used to observe the Higgs decaying into beauty quarks $h \rightarrow b\bar{b}$ by both ATLAS and CMS [48, 49]. Hence, the Vh Higgs production channel is one of the important channels to look for in the future runs of the LHC for better measurement of the VVh coupling as well as Higgs coupling to the beauty quark. As the statistical and systematic uncertainties coming from the experimental setup of the LHC get reduced in the future runs, due to higher integrated luminosity and upgraded detectors and analysis techniques. There is a need to reduce theoretical uncertainties emerging from the perturbative calculations of cross-sections. In order to achieve that, one should include more terms in the perturbative expansion in the couplings, particularly the strong coupling α_s . In this chapter, we are interested in the channel $pp \rightarrow Zh$, which is quark-initiated tree-level process at LO interpreted as **Drell-Yan process** [50, 51]. This process has been computed up to next-to-next-to-leading-order (NNLO) in QCD ($\sim \alpha_s^2$), and at next-to-leading-order (NLO) in the EW interactions ($\sim \alpha^2$) [52].

Despite arising for the first time at NNLO in perturbation theory to the partonic cross-section, the gluon fusion channel $gg \rightarrow Zh$ has a non-negligible contribution to the hadronic cross-section of $pp \rightarrow Zh$ process, which could reach $> 16\%$ of the total cross-section contribution at 14 TeV [53]. The contribution becomes more significant when looking at large invariant mass bins in the differential cross-section. This is due to the significant abundance of gluons at the LHC for large Q as well as the top quark initiated contribution near the $t\bar{t}$ threshold [54]. The gluon fusion channel has a higher scale uncertainties than the quark induced one, and due to the significant contribution of the former, and the absence of gluon fusion channel for Wh channel, the Zh channel has higher theoretical uncertainties. This motivates NLO calculation of the $gg \rightarrow Zh$ channel in order to reduce these uncertainties and facilitate the precision measurement potential of the Zh channel at the future LHC runs, such as sign and magnitude of the top Yukawa coupling, dipole operators [55] and it can receive additional contributions from new particles [56]. Therefore, better understanding of the SM prediction of the Zh gluon

fusion channel is crucial for both the SM precision measurements of Higgs production within the SM and for testing NP in this channel, e.g. new vector-like leptons.

The leading order (LO) contribution to the $gg \rightarrow ZH$ amplitude, given by one-loop diagrams, was computed exactly in refs.[57, 58]. However, for the NLO, the virtual corrections contain multi-scale two-loop integrals some of which are still not known analytically (for the box diagram). The first computation of the NLO terms has been done by [59] using an asymptotic expansion in the limit $m_t \rightarrow \infty$ and $m_b = 0$, and pointed to a K -factor of about ~ 2 . Later, the computation has been improved via soft gluon resummation, and including NLL terms found in ref.[60], the NLL terms has been matched to the fixed NLO computation of [59].

Finite top-quark-mass effects to $gg \rightarrow ZH$ have been investigated in ref.[61] using a combination of large- m_t expansion (LME) and Padé approximants. In addition, a data-driven method to extract the non-Drell-Yan part of $pp \rightarrow ZH$, which is dominated by the gluon-induced contribution, has been proposed in ref.[62], exploiting the known relation between WH and ZH associated production when only the Drell-Yan component of the two processes is considered. A qualitative study focusing on patterns in the differential distribution has been conducted in ref.[63], where $2 \rightarrow 2$ and $2 \rightarrow 3$ LO matrix elements were merged and matched to improve the description of the kinematics.

Very recently, a new analytic computation of the NLO virtual contribution based on a high-energy expansion of the amplitude, supported by Padé approximants, and on an improved LME, has been carried out [64]. The results are in agreement with a new exact numerical study [65], in the energy regions where the expansions are legitimate. Nonetheless, an improvement on the analytic calculation is still desirable, since the heavy-top and the high-energy expansions do not cover well the region $350 \text{ GeV} \lesssim \sqrt{\hat{s}} \lesssim 750 \text{ GeV}$, where $\sqrt{\hat{s}}$ is the partonic center of mass energy. It should be remarked that this region provides a significant part of the hadronic cross section at the LHC, about 68%.

In this paper, we present an analytic calculation of the virtual NLO QCD corrections to the $gg \rightarrow ZH$ process that covers the region $\sqrt{\hat{s}} \lesssim 750 \text{ GeV}$, which contributes about 98% to the hadronic cross section. The most difficult parts, i.e. the two-loop box diagrams, are computed in terms of a forward kinematics [66] via an expansion in the Z (or Higgs) transverse momentum, p_T , while the rest of the virtual corrections is computed exactly. We remark that our calculation is complementary to the results of ref.[64], which covers the region of large transverse momentum of the Z . Furthermore, the merging of the two analyses allows an analytic evaluation of the NLO virtual corrections in $gg \rightarrow ZH$ in the entire phase space.

6.2 Definitions

In this section we introduce our definitions for the calculation of the NLO QCD corrections to the associated production of a Higgs and a Z boson from gluon fusion.

The amplitude $g_a^\mu(p_1)g_b^\nu(p_2) \rightarrow Z^\rho(p_3)H(p_4)$ can be written as

$$\mathcal{A} = i\sqrt{2}\frac{m_Z G_F \alpha_S(\mu_R)}{\pi} \delta_{ab} \epsilon_\mu^a(p_1) \epsilon_\nu^b(p_2) \epsilon_\rho(p_3) \hat{\mathcal{A}}^{\mu\nu\rho}(p_1, p_2, p_3), \quad (6.1)$$

$$\hat{\mathcal{A}}^{\mu\nu\rho}(p_1, p_2, p_3) = \sum_{i=1}^6 \mathcal{P}_i^{\mu\nu\rho}(p_1, p_2, p_3) \mathcal{A}_i(\hat{s}, \hat{t}, \hat{u}, m_t, m_H, m_Z), \quad (6.2)$$

where G_F is the Fermi constant, $\alpha_S(\mu_R)$ is the strong coupling constant defined at a scale μ_R and $\epsilon_\mu^a(p_1)\epsilon_\nu^b(p_2)\epsilon_\rho(p_3)$ are the polarization vectors of the gluons and the Z boson, respectively. The tensors $\mathcal{P}_i^{\mu\nu\rho}$ are a set of orthogonal projectors, whose explicit expressions are presented in appendix A.1. The corresponding form factors $\mathcal{A}_i(\hat{s}, \hat{t}, \hat{u}, m_t, m_H, m_Z)$ are functions of the masses of the top quark (m_t), Higgs (m_H) and Z (m_Z) bosons, and of the partonic Mandelstam variables

$$\hat{s} = (p_1 + p_2)^2, \quad \hat{t} = (p_1 + p_3)^2, \quad \hat{u} = (p_2 + p_3)^2, \quad (6.3)$$

where $\hat{s} + \hat{t} + \hat{u} = m_Z^2 + m_H^2$ and we took all the momenta to be incoming.

The \mathcal{A}_i form factors can be expanded up to NLO terms as

$$\mathcal{A}_i = \mathcal{A}_i^{(0)} + \frac{\alpha_S}{\pi} \mathcal{A}_i^{(1)} \quad (6.4)$$

and the Born partonic cross section can be written as

$$\hat{\sigma}^{(0)}(\hat{s}) = \frac{m_Z^2 G_F^2 \alpha_S(\mu_R)^2}{64 \hat{s}^2 (2\pi)^3} \int_{\hat{t}^-}^{\hat{t}^+} d\hat{t} \sum_i |\mathcal{A}_i^{(0)}|^2, \quad (6.5)$$

where $\hat{t}^\pm = [-\hat{s} + m_H^2 + m_Z^2 \pm \sqrt{(\hat{s} - m_H^2 - m_Z^2)^2 - 4m_H^2 m_Z^2}]/2$.

The Feynman diagrams that contribute to the $gg \rightarrow ZH$ amplitude up to NLO can be separated into triangle, box and double-triangle contributions, the last type appearing for the first time at the NLO level. Examples of LO (NLO) triangle and box categories are shown in fig.6.1 (a) - (c) ((d) - (f)). Due to the presence of a γ_5 in the axial coupling of the Z boson to the fermions in the loop, the projectors $\mathcal{P}_i^{\mu\nu\rho}$ are proportional to the Levi-Civita total anti-symmetric tensor $\epsilon^{\alpha\beta\gamma\delta}$ (see appendix A.1), whose treatment in dimensional regularization is, as well known, delicate and will be discussed in section 6.7.

In our calculation we treat all the quarks but the top as massless. As a consequence, the contribution to the amplitude of the first two generations vanishes. Concerning the

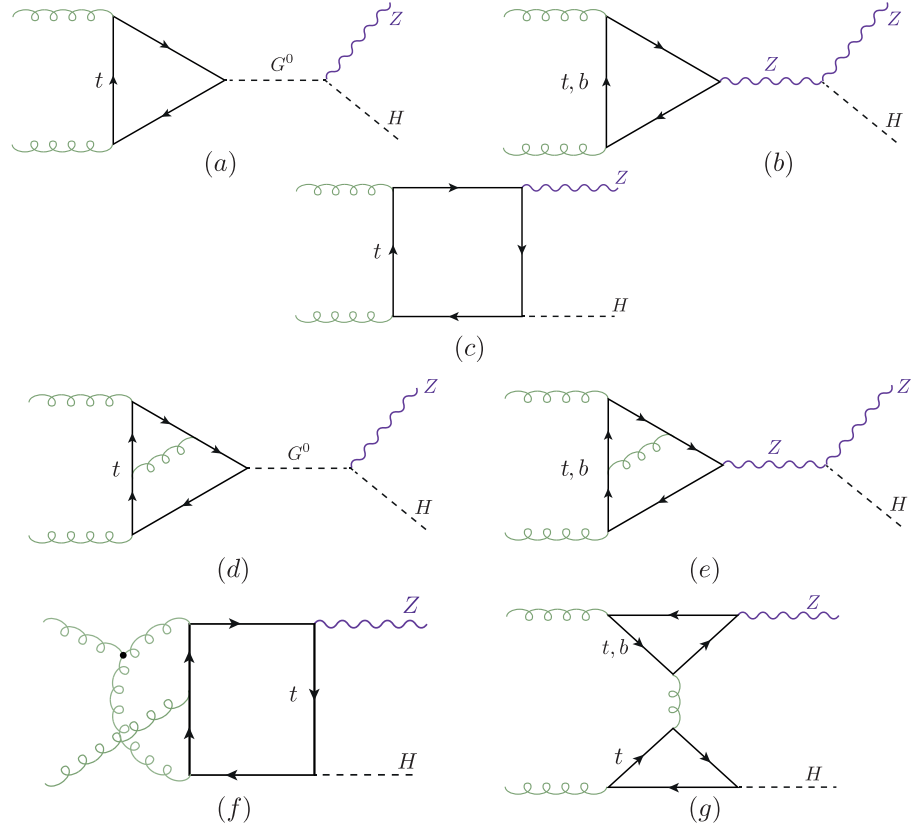


Figure 6.1. Examples of Feynman diagrams contributing to $gg \rightarrow Zh$ at LO and NLO.

third generation, the contribution of the bottom is present in the triangle diagrams with the exchange of a Z boson (fig.6.1(b), (e)) and in the double-triangle diagrams (fig.6.1(g)). A nice observation in ref.[59] allows to compute easily the full (top+bottom) triangle contribution. As noticed in that reference, the triangle contribution with a Z exchange contains a ggZ^* subamplitude which in the Landau gauge can be related to the decay of a massive vector boson with mass $\sqrt{\hat{s}}$ into two massless ones, a process that is forbidden by the Landau-Yang theorem [67, 68]. As a consequence, the full triangle contribution can be obtained from the top triangle diagrams with the exchange of the unphysical scalar G^0 , with the propagator of the G^0 evaluated in the Landau gauge. This part of the top triangle diagrams can be obtained from the decay amplitude of a pseudoscalar boson into two gluons which is known in the literature in the full mass dependence up to NLO terms [69, 70].

Given the above observation, our calculation of the NLO corrections to the $gg \rightarrow ZH$ amplitude focuses on the analytic evaluation of the double-triangle (fig.6.1(g)) and two-loop box contributions (fig.6.1(f)). The former contribution is evaluated exactly. The latter is evaluated via two different expansions: i) via a LME, following ref.[71], up to and including $\mathcal{O}(1/m_t^6)$ terms, which is expected to work below the $2m_t$ threshold; ii) via an expansion in terms of the Z transverse momentum, following ref.[66], whose details are presented in the next section.

6.3 Expansion in the transverse momentum

The transverse momentum of the Z boson can be written in terms of the Mandelstam variables as

$$p_T^2 = \frac{\hat{t}\hat{u} - m_Z^2 m_H^2}{\hat{s}}. \quad (6.6)$$

From eq.(6.6), together with the relation between the Mandelstam variables, one finds

$$p_T^2 + \frac{m_H^2 + m_Z^2}{2} \leq \frac{\hat{s}}{4} + \frac{\Delta_m^2}{\hat{s}}, \quad (6.7)$$

where $\Delta_m = (m_H^2 - m_Z^2)/2$. Eq.(6.7) implies $p_T^2/\hat{s} < 1$ that, together with the kinematical constraints $m_H^2/\hat{s} < 1$ and $m_Z^2/\hat{s} < 1$, allows the expansion of the amplitude in terms of these three ratios.

A direct expansion in p_T is not possible at amplitude level, since p_T itself does not appear in the amplitudes. However, as we argued in ref.[66], the expansion in $p_T^2/\hat{s} \ll 1$ is equivalent to an expansion in terms of the ratio of the reduced Mandelstam variables $t'/s' \ll 1$ or $u'/s' \ll 1$, depending whether we are considering the process to be in a

forward or backward kinematics. The s' , t' and u' variables are defined as

$$s' = p_1 \cdot p_2 = \frac{\hat{s}}{2}, \quad t' = p_1 \cdot p_3 = \frac{\hat{t} - m_Z^2}{2}, \quad u' = p_2 \cdot p_3 = \frac{\hat{u} - m_Z^2}{2} \quad (6.8)$$

and satisfy

$$s' + t' + u' = \Delta_m. \quad (6.9)$$

The cross section of a $2 \rightarrow 2$ process can always be expanded into a forward and backward contribution. Looking at the dependence of σ upon t' , u' we can write

$$\begin{aligned} \sigma &\propto \int_{t_i}^{t_f} dt' \mathcal{F}(t', u') = \int_{t_i}^{t_m} dt' \mathcal{F}(t', u') + \int_{t_m}^{t_f} dt' \mathcal{F}(t', u') \\ &\sim \int_{t_i}^{t_m} dt' \mathcal{F}(t' \sim 0, u' \sim -s') + \int_{t_m}^{t_f} dt' \mathcal{F}(t' \sim -s', u' \sim 0) \end{aligned} \quad (6.10)$$

where $t_i = (\hat{t}^- - m_Z^2)/2$, $t_f = (\hat{t}^+ - m_Z^2)/2$ and t_m is the value of t' at which $t' = u' = (-s' + \Delta_m)/2$. The two terms in the second line of eq.(6.10) represent the expansion in the forward and backward kinematics, respectively.

If the amplitude is symmetric under $t' \leftrightarrow u'$ exchange then

$$\begin{aligned} \sigma &\propto \int_{t_i}^{t_m} dt' \mathcal{F}(0, -s') + \int_{t_m}^{t_f} dt' \mathcal{F}(-s', 0) = \\ &\int_{t_i}^{t_m} dt' \mathcal{F}(0, -s') + \int_{t_m}^{t_f} dt' \mathcal{F}(0, -s') = \int_{t_i}^{t_f} dt' \mathcal{F}(0, -s') \end{aligned} \quad (6.11)$$

so that the expansion in the forward kinematics actually covers the entire phase space.

In the case of $gg \rightarrow ZH$ the process itself is not symmetric under the $t' \leftrightarrow u'$ exchange. However, as can be seen from the explicit expressions of the projectors in appendix A.1, it can be written as a sum of symmetric and antisymmetric form factors. To perform only the expansion in the forward kinematics one can proceed in the following way. On the symmetric form factors the expansion can be directly performed. For the antisymmetric ones, it is sufficient first to extract the overall antisymmetric factor $(\hat{t} - \hat{u})$ just by multiplying the form factor by $1/(\hat{t} - \hat{u})$, written as $1/(2s' - 4t' - 2\Delta_m)$, then perform the expansion in the forward kinematics and finally multiply back by $(\hat{t} - \hat{u})$.

As discussed in ref.[66], to implement the p_T -expansion at the level of Feynman diagrams it is convenient to introduce the vector $r^\mu = p_1^\mu + p_3^\mu$, which satisfies

$$r^2 = \hat{t}, \quad r \cdot p_1 = \frac{\hat{t} - m_Z^2}{2}, \quad r \cdot p_2 = -\frac{\hat{t} - m_H^2}{2}, \quad (6.12)$$

and therefore can be also written as

$$r^\mu = -\frac{\hat{t} - m_H^2}{\hat{s}} p_1^\mu + \frac{\hat{t} - m_Z^2}{\hat{s}} p_2^\mu + r_\perp^\mu = \frac{t'}{s'} (p_2^\mu - p_1^\mu) - \frac{\Delta_m}{s'} p_1^\mu + r_\perp^\mu, \quad (6.13)$$

where

$$r_\perp^2 = -p_T^2. \quad (6.14)$$

From eq.(6.6) one obtains

$$t' = -\frac{s'}{2} \left\{ 1 - \frac{\Delta_m}{s'} \pm \sqrt{\left(1 - \frac{\Delta_m}{s'}\right)^2 - 2\frac{p_T^2 + m_Z^2}{s'}} \right\} \quad (6.15)$$

that implies that the expansion in small p_T (the minus sign case in eq.(6.15)) can be realized at the level of Feynman diagrams, by expanding the propagators in terms of the vector r^μ around $r^\mu \sim 0$ or, equivalently, $p_3^\mu \sim -p_1^\mu$, see eq.(6.13).

The outcome of the evaluation of the $gg \rightarrow ZH$ amplitude via a p_T -expansion is expressed in terms of a series of Master Integrals (MIs) that are functions of \hat{s} and m_t^2 only, and whose coefficients can be organized in terms of powers of ratios of small over large parameters where p_T^2 , m_H^2 and m_Z^2 are identified as the small parameters while m_t^2 and \hat{s} as the large ones. Thus, the range of validity of the expansion depends on the condition that p_T^2 can be treated as a “small parameter” with respect to m_t^2 because all the other ratios, small over large, are always smaller than 1.

6.4 LO Comparison

In order to investigate the range of validity of the evaluation of the $gg \rightarrow ZH$ amplitude via a p_T -expansion, we compare the exact result for the LO partonic cross section [57, 58] with the result obtained via our p_T -expansion. The latter is expressed in terms of the same four MIs that enter into the analogous calculation of the $gg \rightarrow HH$ LO amplitude [66], or

$$B_0[\hat{s}, m_t^2, m_t^2] \equiv B_0^+, \quad B_0[-\hat{s}, m_t^2, m_t^2] \equiv B_0^-, \quad (6.16)$$

$$C_0[0, 0, \hat{s}, m_t^2, m_t^2, m_t^2] \equiv C_0^+, \quad C_0[0, 0, -\hat{s}, m_t^2, m_t^2, m_t^2] \equiv C_0^- \quad (6.17)$$

where

$$B_0[q^2, m_1^2, m_2^2] = \frac{1}{i\pi^2} \int \frac{d^n k}{\mu^{n-4}} \frac{1}{(k^2 - m_1^2)((k+q)^2 - m_2^2)} \quad (6.18)$$

$$C_0[q_a^2, q_b^2, (q_a + q_b)^2, m_1^2, m_2^2, m_3^2] = \frac{1}{i\pi^2} \int \frac{d^n k}{\mu^{n-4}} \frac{1}{[k^2 - m_1^2][(k + q_a)^2 - m_2^2][(k - q_b)^2 - m_3^2]} \quad (6.19)$$

are the Passarino-Veltman functions [72], with n the dimension of spacetime and μ the 't Hooft mass.

As an illustration of our LO result we present the explicit expressions for one symmetric, \mathcal{A}_2 , and one antisymmetric, \mathcal{A}_6 , form factor including the first correction in the ratio of small over large parameters which will be referred to as¹ $\mathcal{O}(p_T^2)$. We divide the result into triangle (\triangle) and box (\square) contribution or

$$\begin{aligned} \mathcal{A}_2^{(0,\triangle)} &= -\frac{p_T}{\sqrt{2}(m_Z^2 + p_T^2)}(\hat{s} - \Delta_m) m_t^2 C_0^+, \\ \mathcal{A}_2^{(0,\square)} &= \frac{p_T}{\sqrt{2}(m_Z^2 + p_T^2)} \left\{ \begin{aligned} &\left(m_t^2 - m_Z^2 \frac{\hat{s} - 6m_t^2}{4\hat{s}} - p_T^2 \frac{12m_t^4 - 16m_t^2\hat{s} + \hat{s}^2}{12\hat{s}^2} \right) B_0^+ \\ &- \left(m_t^2 - \Delta_m \frac{m_t^2}{(4m_t^2 + \hat{s})} + m_Z^2 \frac{24m_t^4 - 6m_t^2\hat{s} - \hat{s}^2}{4\hat{s}(4m_t^2 + \hat{s})} - \right. \\ &\quad \left. p_T^2 \frac{48m_t^6 - 68m_t^4\hat{s} - 4m_t^2\hat{s}^2 + \hat{s}^3}{12\hat{s}^2(4m_t^2 + \hat{s})} \right) B_0^- \\ &+ \left(2m_t^2 - \Delta_m + m_Z^2 \frac{3m_t^2 - \hat{s}}{\hat{s}} + p_T^2 \frac{3m_t^2\hat{s} - 2m_t^4}{\hat{s}^2} \right) m_t^2 C_0^- \\ &+ \left(\hat{s} - 2m_t^2 + m_Z^2 \frac{\hat{s} - 3m_t^2}{\hat{s}} + p_T^2 \frac{2m_t^4 - 3m_t^2\hat{s} + \hat{s}^2}{\hat{s}^2} \right) m_t^2 C_0^+ \\ &+ \log\left(\frac{m_t^2}{\mu^2}\right) \frac{m_t^2}{(4m_t^2 + \hat{s})} \left(\Delta_m + 2m_Z^2 + p_T^2 \frac{2\hat{s} - 2m_t^2}{3\hat{s}} \right) \\ &- \Delta_m \frac{2m_t^2}{(4m_t^2 + \hat{s})} + m_Z^2 \frac{\hat{s} - 12m_t^2}{4(4m_t^2 + \hat{s})} + p_T^2 \frac{8m_t^4 - 2m_t^2\hat{s} + \hat{s}^2}{4\hat{s}(4m_t^2 + \hat{s})} \end{aligned} \right\}, \end{aligned} \quad (6.21)$$

¹With a slight abuse of notation we indicate the counting of the orders in the expansion as $\mathcal{O}(p_T^{2n})$ that actually means the inclusion of terms that scale as $(x/y)^n$, where $x = p_T^2, m_Z^2, m_H^2$ and $y = \hat{s}, m_t^2$, with respect to the $\hat{s}, m_t^2 \rightarrow \infty$ contribution. The latter is indicated as $\mathcal{O}(p_T^0)$ and corresponds to the first non zero contribution in the expansion of the diagrams in terms of the vector r^μ .

and

$$\mathcal{A}_6^{(0,\Delta)} = 0, \quad (6.22)$$

$$\begin{aligned} \mathcal{A}_6^{(0,\square)} &= \frac{\hat{t} - \hat{u}}{\hat{s}^2} p_T \left[\frac{m_t^2}{2} (B_0^- - B_0^+) - \frac{\hat{s}}{4} \right. \\ &\quad \left. - \frac{2m_t^2 + \hat{s}}{2} m_t^2 C_0^- + \frac{2m_t^2 - \hat{s}}{2} m_t^2 C_0^+ \right], \end{aligned} \quad (6.23)$$

where in eqs.(6.21,6.23) the B_0 functions are understood as the finite part of the integrals on the right hand side of eq.(6.18).

In fig.6.2 the exact partonic LO cross section (red line) is shown as a function of the invariant mass of the ZH system, M_{ZH} , and compared to various p_T -expanded results. For the numerical evaluation of the cross section here and in the following, we used as SM input parameters

$$\begin{aligned} m_Z &= 91.1876 \text{ GeV}, \quad m_H = 125.1 \text{ GeV}, \quad m_t = 173.21 \text{ GeV}, \\ m_b &= 0 \text{ GeV}, \quad G_F = 1.16637 \text{ GeV}^{-2}, \quad \alpha_s(m_Z) = 0.118. \end{aligned}$$

In the lower part of fig.6.2 the ratio of the exact result over the p_T -expanded one is shown. From this ratio one can see that the $\mathcal{O}(p_T^0)$ contribution covers well the ZH invariant mass region $M_{ZH} \lesssim 2m_t$, corresponding to the range of validity of an expansion in the large top quark mass. Furthermore, when the contributions up to $\mathcal{O}(p_T^4)$ are taken into account a remarkable agreement with the exact result is found up to $M_{ZH} \lesssim 750 \text{ GeV}$. This agreement is extended to slightly higher values of M_{ZH} when the $\mathcal{O}(p_T^6)$ contribution is included, a finding in close analogy to the result for di-Higgs production [66]. Similar conclusions can be drawn from table 6.1, where it is shown that the partonic cross section at $\mathcal{O}(p_T^4)$ agrees with the full result for $M_{ZH} \lesssim 600 \text{ GeV}$ on the permille level and the agreement further improves when $\mathcal{O}(p_T^6)$ terms are included. As a final remark for this section, we notice that, from the comparison with the LO exact result, the p_T -expanded evaluation of the amplitude is expected to provide an accurate result up to $M_{ZH} \sim 700 - 750 \text{ GeV}$ that corresponds, from eq.(6.7), to $p_T \lesssim 300 - 350 \text{ GeV} \approx 2m_t$.

6.5 Renormalisation

Recall that the bare amplitude reads :

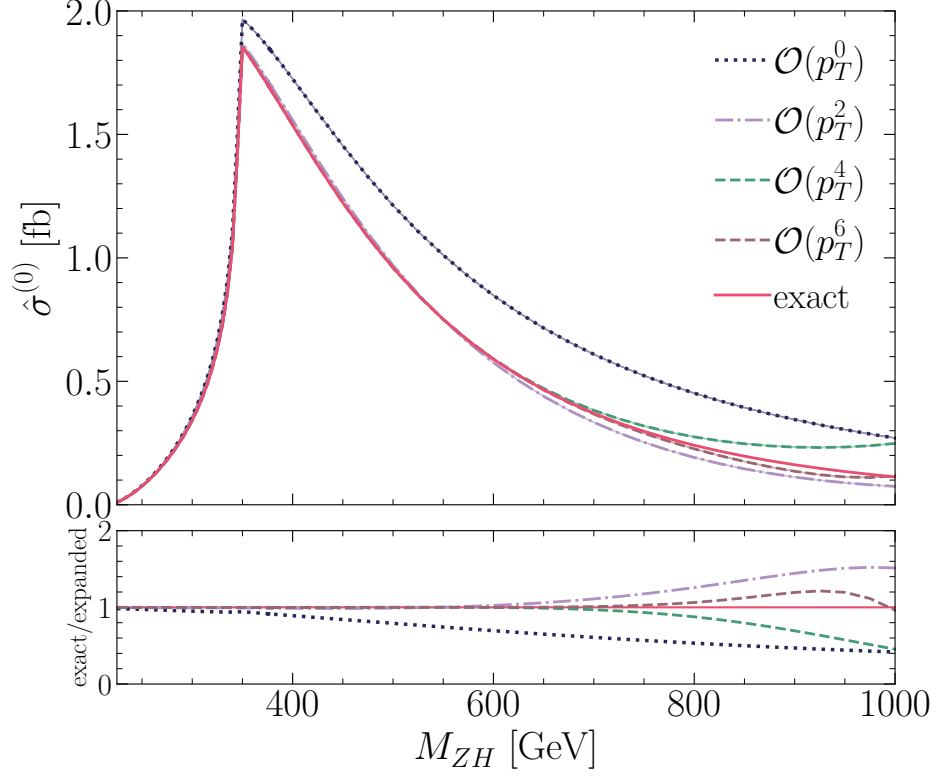


Figure 6.2. LO partonic cross section as a function of the invariant mass M_{ZH} . The full result (red line) is plotted together with results at different orders in the p_T -expansion (dashed lines). In the bottom part, the ratio of the full result over the p_T -expanded one at various orders is shown.

$$\begin{aligned}
 -i\mathcal{M} &= \varepsilon_\mu(p_1)\varepsilon_\nu(p_2) T_R \delta_{ab} \mu_R^{2\epsilon} \alpha_S \hat{\mathcal{P}}_{\mu\nu\rho} \\
 &\times S_\epsilon \left(\frac{\mu_R^2}{\hat{s}} \right)^\epsilon \left[\mathcal{F}^{1\ell} + \mu_R^{2\epsilon} \alpha_S \mu_R^{-2\epsilon} S_\epsilon \left(\frac{\mu_R^2}{\hat{s}} \right)^\epsilon \mathcal{F}^{2\ell} \right]
 \end{aligned} \tag{6.24}$$

M_{ZH} [GeV]	$\mathcal{O}(p_T^0)$	$\mathcal{O}(p_T^2)$	$\mathcal{O}(p_T^4)$	$\mathcal{O}(p_T^6)$	full
300	0.3547	0.3393	0.3373	0.3371	0.3371
350	1.9385	1.8413	1.8292	1.8279	1.8278
400	1.6990	1.5347	1.5161	1.5143	1.5142
600	0.8328	0.5653	0.5804	0.5792	0.5794
750	0.5129	0.2482	0.3129	0.2841	0.2919

Table 6.1. The partonic cross section $\hat{\sigma}^{(0)}$ at various orders in p_T and the full computation for several values of M_{ZH} .

Where $\mathcal{F}^{n\ell}$ is the nth loop form factor, and $\hat{\mathcal{P}}_{\mu\nu\rho}$ is the normalised projector, written as

$$\begin{aligned}
L_{\mu\nu\rho}^{(1)} &= \frac{\hat{s}}{2} \varepsilon_{\mu\nu\rho\xi} p_2^\xi - (p_2)_\mu \varepsilon_{\nu\rho\xi\lambda} p_1^\xi p_2^\lambda, \\
L_{\mu\nu\rho}^{(2)} &= \frac{\hat{s}}{2} \varepsilon_{\mu\nu\rho\xi} p_1^\xi - (p_1)_\nu \varepsilon_{\mu\rho\xi\lambda} p_1^\xi p_2^\lambda, \\
\hat{\mathcal{P}}_{\mu\nu\rho} &= \frac{2}{\hat{s}^3} \left(L_{\mu\nu\rho}^{(1)} - L_{\mu\nu\rho}^{(2)} \right).
\end{aligned} \tag{6.25}$$

The 1 loop form factor is given by

$$\mathcal{F}^{1\ell} = \frac{m^2}{\hat{s}} C_0(\hat{s}, 0; m, m, m) - \frac{1}{4\hat{s}}, \tag{6.26}$$

where the last term, not proportional to the mass is corresponding to the chiral anomaly. The 2 loop form-factor, can be decomposed in terms of the colour Casimir invariants C_A and C_F

$$\mathcal{F}^{2\ell} = C_F \mathcal{F}_{CF}^{2\ell} + C_A \mathcal{F}_{CA}^{2\ell} \tag{6.27}$$

The CA part contains double pole $\mathcal{O}(1/\epsilon^2)$ and a single pole $\mathcal{O}(1/\epsilon)$, both coming from the IR divergence. Whilst the CF part contains a UV divergent pole that needs to be cured via mass renormalisation. The poles do not have a dependence on the renormalisation scale μ_R , however, there is a dependence on that scale in the finite part.

6.5.1 Gluon wavefunction

We start by the gluon wavefunction renormalisation of the incoming gluons (external legs) such that the amplitude is renormalised by $Z_A^{1/2}$ for each gluon.

$$Z_A = 1 + \alpha_s \frac{2}{3\epsilon} \left(\frac{\mu_R^2}{m_t^2} \right)^\epsilon. \tag{6.28}$$

6.5.2 Strong coupling constant

The strong couplings constant α_s renormalisation is done via replacing the bare constant α_s^0 with the renormalised one, hence it becomes $\alpha_s^0 = \frac{\mu_R^{2\epsilon}}{S_\epsilon} Z_{\alpha_s} \alpha_s$, where

$$Z_{\alpha_s} = 1 - \frac{\alpha_s}{4\pi} \frac{1}{\epsilon} \left(\beta_0 - \frac{2}{3} \right) \left(\frac{\mu_R^2}{m_t^2} \right)^\epsilon, \quad (6.29)$$

and the constant $\beta_0 = \frac{11}{3}C_A - \frac{2}{3}N_f$, where N_f is the number of "active" flavours. In the 5-flavour scheme $N_f = 5$.

6.5.3 Top mass

We use the \overline{MS} scheme for the top mass renormalisation $m_0 = Z_m m$, replaced in the propagators, also can be done with multiplying δZ_m with the derivative of the 1 loop form-factor with respect to the mass., here Z_m is given by

$$Z_m = 1 + C_F \frac{3}{\epsilon}. \quad (6.30)$$

For the on-shell scheme we add the finite renormalisation term

$$Z_m^{OS} = 1 - 2C_F \quad (6.31)$$

6.5.4 Larin counter-term

For the vertex $-i\bar{\psi}\gamma_\rho\gamma_5\psi$, we let γ_5 naively anti-commute with all d -dimensional γ_μ 's and then correct that with the finite renormalisation constant

$$Z_5 = 1 - 2C_F \quad (6.32)$$

6.5.5 All terms together

The renormalised amplitude is written as

$$\mathcal{M}(\alpha_s, m, \mu_R) = Z_A \mathcal{M}(\alpha_s^0, m^0). \quad (6.33)$$

Putting all the above substitutions together, we get the renormalised 2 loop form-factor:

$$(\mathcal{F}^{2\ell})^R = \mathcal{F}^{2\ell} - \mathcal{F}_{UV}^{1\ell} - \mathcal{F}_{UV,m}^{1\ell} + \mathcal{F}_{\text{Larin}}^{1\ell} \quad (6.34)$$

$$\begin{aligned} \mathcal{F}_{UV}^{1\ell} &= \frac{\alpha_s}{4\pi} \frac{\beta_0}{\epsilon} \left(\frac{\mu_R^2}{\hat{s}} \right)^{-\epsilon} \\ \mathcal{F}_{UV,m}^{1\ell} &= \frac{\alpha_s}{4\pi} \left(\frac{3}{\epsilon} - 2 \right) C_F \left(\frac{\mu_R^2}{\hat{s}} \right)^{-\epsilon} m^0 \partial_m \mathcal{F}^{1\ell}. \end{aligned} \quad (6.35)$$

$$\mathcal{F}_{\text{Larin}}^{1\ell} = -\frac{\alpha_s}{4\pi} C_F \mathcal{F}^{1\ell}.$$

We expand the 1 loop for factor up to order $\mathcal{O}(\epsilon)$.

6.6 IR subtraction

We use the following IR-counter-term

$$\mathcal{F}_{IR}^{1\ell} = \frac{e^{\gamma_E \epsilon}}{\Gamma(1-\epsilon)} \frac{\alpha_s}{4\pi} \left(\frac{\beta_0}{\epsilon} + \frac{C_A}{\epsilon^2} \right) \left(\frac{\mu_R^2}{\hat{s}} \right)^{2\epsilon} \mathcal{F}^{1\ell} \quad (6.36)$$

Here, we expand the 1 loop up to order $\mathcal{O}(\epsilon^2)$.

6.7 Outline of the NLO Computation

In this section we discuss our evaluation of the three different types of diagrams that appear in the virtual corrections to the $gg \rightarrow ZH$ amplitude at the NLO.

The triangle contribution (fig.6.1(d), (e)) was evaluated using the observation of ref.[59], i.e. we adapted the result of ref.[70] for the decay of a pseudoscalar boson into two gluons to our case. This contribution is evaluated exactly and explicit expressions for the form factors are presented in appendix A.2. We notice that if we interpret the exact result in terms of our counting of the expansion in p_T , the p_T -expansion of the triangle contribution stops at $\mathcal{O}(p_T^2)$.

Given the reducible structure of the double-triangle diagrams (fig.6.1(g)), an exact result for the double-triangle contribution can be derived in terms of products of one-loop Passarino-Veltman functions [72]. Explicit expressions for this contribution are presented in appendix A.2. Although we write the amplitude using a different tensorial structure with respect to ref.[64] we checked, using the relations between the two tensorial structures reported in appendix A.1, that our result is in agreement with the one presented in ref.[61].

The box contribution (fig.6.1(f)) was computed evaluating the two-loop multi-scale Feynman integrals via two different expansions: a LME up to and including $\mathcal{O}(1/m_t^6)$ terms, and an expansion in the transverse momentum up to and including $\mathcal{O}(p_T^4)$ terms. The former expansion was used as “control” expansion of the latter. Indeed, the p_T -expanded result actually “contains” the LME one. The LME differs from the expansion in p_T by the fact that \hat{s} is treated as a small parameter with respect to m_t^2 , and not on the same footing as in the latter case. This implies that if the p_T -expanded result is further expanded in terms of the \hat{s}/m_t^2 ratio the LME result has to be recovered. This way, we were able to reproduce, at the analytic level, our LME result.

We conclude this section outlining some technical details concerning our computation. We generated the amplitudes using `FeynArts` [73] and contracted them with the projectors as defined in appendix A.1 using `FeynCalc` [74, 75] and in-house Mathematica routines. We used dimensional regularization and the rule for the contraction of two epsilon tensors written in terms of the determinant of n -dimensional metric tensors. This is not a consistent procedure and needs to be corrected. A correction term should be added [76] to the form factors computed as described above, $\mathcal{A}_i^{(1,ndr)}$, namely

$$\mathcal{A}_i^{(1)} = \mathcal{A}_i^{(1,ndr)} - \frac{\alpha_S}{\pi} C_F \mathcal{A}_i^{(0)}. \quad (6.37)$$

In order to check eq.(6.37), following ref.[77] we bypassed the problem of the treatment of γ_5 in dimensional regularization computing the amplitude via a LME working in 4 dimension, employing the Background Field Method (BFM) [78] and using as regularization scheme the Pauli-Villars method. This result was compared with the LME evaluation of $\mathcal{A}_i^{(1,ndr)}$, finding that the difference between the two evaluations was indeed given by the second term on the right-hand-side of eq.(6.37).

After the contraction of the epsilon tensors the diagrams were expanded as described in section 6.3. They were reduced to MIs using `FIRE` [79] and `LiteRed` [80]. The resulting MIs were exactly the same as previously found for di-Higgs production [66]. Nearly all of them are expressed in terms of generalised harmonic polylogarithms with the exception of two elliptic integrals [81, 82]. The top quark mass was renormalized in the onshell scheme² and the IR poles were subtracted as in ref.[83].

6.8 Conclusion

In this paper, we computed the two-loop NLO virtual corrections to the $gg \rightarrow ZH$ process. Among the two-loop Feynman diagrams contributing to the process, the ones belonging to the triangle and double-triangle topology were computed exactly. The ones belonging to the box topology, which contain multiscale integrals, were evaluated via an expansion in the Z transverse momentum. This novel approach of computing a process

²Different choices for the renormalized top mass can be easily implemented in our calculation.

in the forward kinematics was originally proposed in ref.[66] for double Higgs production where the particles in the final state have the same mass. In this paper, we extended the method to the more general case of two different masses in the final state and to a process whose amplitude is not symmetric under the $\hat{t} \leftrightarrow \hat{u}$ exchange.

The result of the evaluation of the box contribution is expressed, both at one- and two-loop level, in terms of the same set of MIs that was found in ref.[66] for double Higgs production. The two-loop MIs can be all expressed in terms of generalised harmonic polylogarithms with the exception of two elliptic integrals.

As we have shown explicitly at the LO, the range of validity of our computation covers values of the invariant mass $M_{ZH} \lesssim 750$ GeV corresponding to 98.5% of the phase space at LHC energies. We showed that few terms in our expansion were sufficient to obtain an incredible good agreement with the numerical evaluation of \mathcal{V}_{fin} presented in ref.[65], at the level of a permille or less difference between our analytic result and the numerical one.

The advantage of our analytic approach compared to the numerical calculation is also in the computing time. With an average evaluation time of half a second per phase space point, an inclusion into a Monte Carlo programme is realistic. Due to the flexibility of our analytic results, an application to beyond-the-Standard Model is certainly possible.

Finally, we remark that our calculation complements nicely the results obtained in ref.[64] using a high-energy expansion, that according to the authors provides precise results for $p_T \gtrsim 200$ GeV. The merging of the two analyses is going to provide a result that covers the whole phase space, can be easily implemented into a Monte Carlo code and presents the flexibility of an analytic calculation.

Part III

Higgs Pair at Hadron Colliders

7 Overview of Higgs pair production at colliders

The dominant process for Higgs pair production at the LHC (and hadron colliders in general) is the gluon gluon fusion (ggF) via a heavy quark loop Q , mainly the top and beauty quark, with the latter contributing only to about 1%, see figure 7.1. This

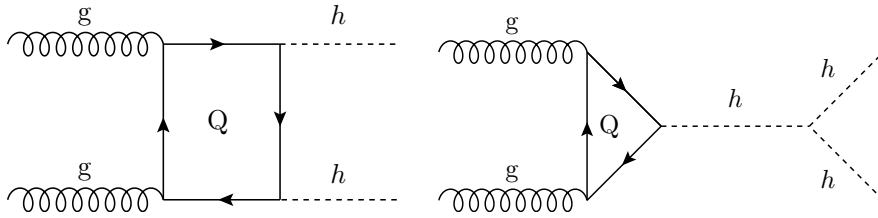


Figure 7.1. Feynman diagrams for the ggF process of Higgs pair production in the SM.

process is well-studied at leading order (LO) analytically [84, 85, 86, 87]. The next-to-leading QCD order (NLO) was initially computed using infinite top mass limit ($m_t \rightarrow \infty$) using the Higgs effective field theory (HEFT) and implemented in the programme **Hpair** [88]. However, this approximation is not suitable for obtaining distributions, and using numerical methods [89, 90, 91] the full NLO results were obtained. In [92], parton shower effects were included in the NLO calculations, allowing the use of the NLO in event generators such as PYTHIA and POWHEG. Analytical calculations for the NLO corrections using small Higgs transverse momentum $p_{T,h} \rightarrow 0$ yielded a good estimation for the numerical result [66]. The use of Padé approximation obtained also analytical results for the NLO result and a description for the three-loop (NNLO) form factors [93]. The NNLO cross section with top mass effects has been computed numerically in [94].

In this work, we have calculated the $\sqrt{s} = 14$ TeV LO ggF inclusive cross-section and distributions with modified light Yukawa couplings by including the light quark loops and the coupling $hhq\bar{q}$ described in the last diagram in figure 7.2. The calculation was carried out using a FORTRAN code utilising the VEGAS integration algorithm, and NNPDF30 parton distribution functions (PDF's)[95] implemented via LHAPDF-6 package[96]. For the loop integrals (see Appendix), we have used the COLLIER library [97] for regularisation of the IR divergent light quark loops, that were assumed massless. A K -factor, for the NNLO correction were used according to the Higgs cross section working group

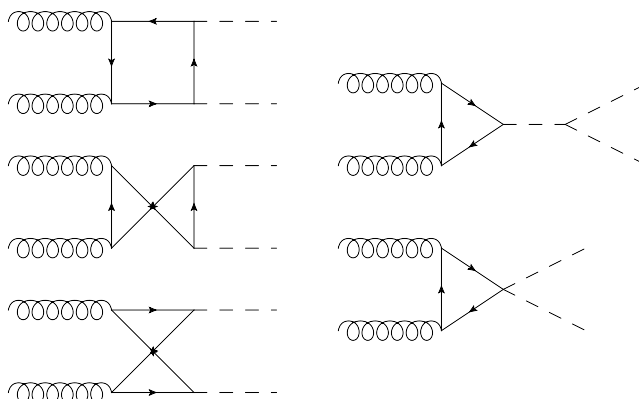


Figure 7.2. The one-loop diagrams calculated in the ggF with modified Yukawa couplings

recommended values [98, 99]:

$$K = \frac{\sigma_{NNLO}}{\sigma_{LO}}, \quad K_{14\text{TeV}} \approx 1.71. \quad (7.1)$$

Since the cross-section is not expected to change a lot by changing the light Yukawa couplings, we use the same NNLO K-factor for all values of the scalings. The renormalisation μ_R and factorisation μ_F scales of the α_s and PDF running are set to $\mu_0 = 0.5 M_{hh}$, and $\alpha_s(M_Z) = 0.118$. In our calculations, we did not consider the quark mass running, as the later will be accounted for in the K-factor.

Theoretical systematic uncertainties

There are three main sources of theoretical *systematic* uncertainties:

1. Scale uncertainty: coming from the arbitrariness of scales choice.
2. PDF uncertainties : coming from the uncertainty in the PDF fitting and model.
3. α_s running uncertainty: originating from the initial value (i.e. $\alpha_s(M_Z)$).

In order to compute these uncertainties, we follow the recommendations of the Higgs cross-section working group for the value and uncertainty of α_s

$$\alpha_s(M_Z) = 0.1180 \pm 0.0015, \quad (7.2)$$

and the methods described in [100, 101]. for PDF and α_s uncertainties. In order to calculate the scale uncertainties, the cross-section was computed with different μ_R and

	σ [fb]	Scale [fb]	PDF+ α_s [fb]	Total [fb]
SM HEFT (LO)	18.10	—	—	—
SM running mass (LO)	16.96	—	—	—
SM (LO)	21.45	+4.29 −3.43	± 1.46	+4.53 −3.73
SM (NLO) [102]	33.89	+6.17 −4.98	+2.37 −2.01	+6.61 −5.37
SM (NNLO) [94]	36.69	+0.77 −1.83	± 1.10 ($g_{hq\bar{q}} = g_{hb\bar{b}}^{SM}$)	+1.66 −6.43 (incl. m_t uncertainty)
($g_{hq\bar{q}} = g_{hb\bar{b}}^{SM}$) (ggF-LO)	21.84	+4.38 −3.51	± 1.49	+4.62 −3.81

Table 7.1. Gluon fusion (ggF) Higgs pair production cross-section with theoretical systematic uncertainties, for infinite top mass limit (SM HEFT), running mass, LO, NLO and NNLO QCD corrections. The NLO and NNLO results are taken from the references cited in the table. We also state the benchmark point ($g_{hq\bar{q}} = g_{hb\bar{b}}^{SM}$) cross section result (all the light Yukawa couplings are scaled to the SM beauty Yukawa)

μ_F values ranging between:

$$\frac{M_{hh}}{4} \leq \mu_R/\mu_F \leq M_{hh} \quad (7.3)$$

The scale uncertainty for the LO total cross-section was found to be +20%, −16%. Moreover, the PDF+ α_s uncertainty was $\pm 6.8\%$.

results

The total cross sections with their uncertainties is shown in table ??.

8 Higgs pair as a probe for light Yukawas

9 Optimised search for Higgs pair via Interpretable machine learning

A Details of Zh calculation

A.1 Orthogonal Projectors in $gg \rightarrow ZH$

In this appendix we present the explicit expressions of the projectors $\mathcal{P}_i^{\mu\nu\rho}$ appearing in eq.(6.2). The projectors are all normalized to 1. They are:

$$\mathcal{P}_1^{\mu\nu\rho} = \frac{m_Z}{\sqrt{2}s'p_T^2} \left[p_1^\nu \epsilon^{\mu\rho p_1 p_2} - p_2^\mu \epsilon^{\nu\rho p_1 p_2} + q_t^\mu \epsilon^{\nu\rho p_2 p_3} \right. \quad (\text{A.1})$$

$$\left. + q_u^\nu \epsilon^{\mu\rho p_1 p_3} + s' \epsilon^{\mu\nu\rho p_2} - s' \epsilon^{\mu\nu\rho p_1} \right], \quad (\text{A.2})$$

$$\mathcal{P}_2^{\mu\nu\rho} = \frac{1}{\sqrt{2}s'p_T} \left[q_u^\nu \epsilon^{\mu\rho p_1 p_3} + q_t^\mu \epsilon^{\nu\rho p_2 p_3} \right], \quad (\text{A.3})$$

$$\begin{aligned} \mathcal{P}_3^{\mu\nu\rho} &= \frac{\sqrt{3}}{2s'p_T} \left[s' \epsilon^{\mu\nu\rho p_1} + s' \epsilon^{\mu\nu\rho p_2} - p_1^\nu \epsilon^{\mu\rho p_1 p_2} - p_2^\mu \epsilon^{\nu\rho p_1 p_2} \right. \\ &+ (q_u^\nu \epsilon^{\mu\rho p_1 p_3} - q_t^\mu \epsilon^{\nu\rho p_2 p_3}) \left(\frac{1}{3} + \frac{m_Z^2}{p_T^2} \right) \\ &\left. + \frac{m_Z^2}{p_T^2} (q_t^\mu \epsilon^{\nu\rho p_2 p_1} - q_u^\nu \epsilon^{\mu\rho p_1 p_2}) \right], \end{aligned} \quad (\text{A.4})$$

$$\mathcal{P}_4^{\mu\nu\rho} = \frac{m_Z}{\sqrt{2}s'p_T^2} \left[q_t^\mu (\epsilon^{\nu\rho p_2 p_1} - \epsilon^{\nu\rho p_2 p_3}) - q_u^\nu (\epsilon^{\mu\rho p_1 p_2} - \epsilon^{\mu\rho p_1 p_3}) \right], \quad (\text{A.5})$$

$$\mathcal{P}_5^{\mu\nu\rho} = \frac{1}{\sqrt{6}s'p_T} \left[q_t^\mu \epsilon^{\nu\rho p_2 p_3} - q_u^\nu \epsilon^{\mu\rho p_1 p_3} \right], \quad (\text{A.6})$$

$$\begin{aligned} \mathcal{P}_6^{\mu\nu\rho} &= \frac{1}{s'p_T} \left[g^{\mu\nu} \epsilon^{\rho p_1 p_2 p_3} + s' \epsilon^{\mu\nu\rho p_3} + p_1^\nu \epsilon^{\mu\rho p_2 p_3} - p_2^\mu \epsilon^{\nu\rho p_1 p_3} - \frac{s'}{2} \epsilon^{\mu\nu\rho p_2} \right. \\ &+ \frac{1}{2} (p_1^\nu \epsilon^{\mu\rho p_1 p_2} + p_2^\mu \epsilon^{\nu\rho p_1 p_2} + q_u^\nu \epsilon^{\mu\rho p_1 p_3} - q_t^\mu \epsilon^{\nu\rho p_2 p_3} - s' \epsilon^{\mu\nu\rho p_1}) \\ &\left. + \frac{m_Z^2}{2p_T^2} (q_t^\mu \epsilon^{\nu\rho p_2 p_1} - q_u^\nu \epsilon^{\mu\rho p_1 p_2} + q_u^\nu \epsilon^{\mu\rho p_1 p_3} - q_t^\mu \epsilon^{\nu\rho p_2 p_3}) \right], \end{aligned} \quad (\text{A.7})$$

where we defined $q_t^\mu = (p_3^\mu - \frac{t'}{s'} p_2^\mu)$ and $q_u^\nu = (p_3^\nu - \frac{u'}{s'} p_1^\nu)$ and we used the shorthand notation $\epsilon^{\mu\nu\rho p_2} \equiv \epsilon^{\mu\nu\rho\sigma} p_2^\sigma$.

Using these projectors we obtained the relations between the form factors \mathcal{A}_i defined

in in eq.(6.2) and those defined in section 2 of ref.[64]:

$$\mathcal{A}_1 = \frac{p_T^2}{2\sqrt{2}m_Z(p_T^2 + m_Z^2)} \left[(t' + u')F_{12}^+ - (t' - u')F_{12}^- \right], \quad (\text{A.8})$$

$$\begin{aligned} \mathcal{A}_2 = & -\frac{p_T}{2\sqrt{2}(p_T^2 + m_Z^2)} \left[(t' + u')F_{12}^+ - (t' - u')F_{12}^- \right. \\ & \left. - \frac{p_T^2 + m_Z^2}{2s'} ((t' + u')F_3^+ - (t' - u')F_3^-) \right], \end{aligned} \quad (\text{A.9})$$

$$\begin{aligned} \mathcal{A}_3 = & \frac{p_T}{2\sqrt{3}(p_T^2 + m_Z^2)} \left[(t' + u')F_{12}^- - (t' - u')F_{12}^+ \right. \\ & \left. + (p_T^2 + m_Z^2)(F_2^- + F_4) \right], \end{aligned} \quad (\text{A.10})$$

$$\begin{aligned} \mathcal{A}_4 = & -\frac{m_Z}{2\sqrt{2}(p_T^2 + m_Z^2)} \left[(t' + u')F_{12}^- - (t' - u')F_{12}^+ \right. \\ & \left. + (p_T^2 + m_Z^2) \left(\left(1 - \frac{p_T^2}{m_Z^2}\right) F_2^- + 2F_4 \right) \right], \end{aligned} \quad (\text{A.11})$$

$$\begin{aligned} \mathcal{A}_5 = & \frac{p_T}{2\sqrt{6}(p_T^2 + m_Z^2)} \left[(t' + u')F_{12}^- - (t' - u')F_{12}^+ \right. \\ & \left. + (p_T^2 + m_Z^2) \left(4(F_2^- + F_4) + \frac{3}{2s'} ((t' + u')F_3^- - (t' - u')F_3^+) \right) \right], \end{aligned} \quad (\text{A.12})$$

$$\mathcal{A}_6 = \frac{p_T}{2} F_4. \quad (\text{A.13})$$

A.2 Two-loop Results

The NLO amplitude can be written in terms of three contributions, namely the two-loop 1PI triangle, the two-loop 1PI box and the reducible double-triangle diagrams,

$$\mathcal{A}_i^{(1)} = \mathcal{A}_i^{(1,\triangle)} + \mathcal{A}_i^{(1,\square)} + \mathcal{A}_i^{(1,\bowtie)}. \quad (\text{A.14})$$

We present here the exact results for the double-triangle and triangle contributions to all the form factors. We find

$$\mathcal{A}_1^{(1,\boxtimes)} = -\frac{m_t^2 p_T^2}{4\sqrt{2} m_Z (m_Z^2 + p_T^2)^2} \left[F_t(\hat{t}) \left(G_t(\hat{t}, \hat{u}) - G_b(\hat{t}, \hat{u}) \right) + (\hat{t} \leftrightarrow \hat{u}) \right], \quad (\text{A.15})$$

$$\mathcal{A}_2^{(1,\boxtimes)} = \frac{m_t^2 p_T}{4\sqrt{2} (m_Z^2 + p_T^2)^2} \left[F_t(\hat{t}) \left(G_t(\hat{t}, \hat{u}) - G_b(\hat{t}, \hat{u}) \right) + (\hat{t} \leftrightarrow \hat{u}) \right], \quad (\text{A.16})$$

$$\mathcal{A}_3^{(1,\boxtimes)} = \frac{m_t^2 p_T}{4\sqrt{3} \hat{s} (m_Z^2 + p_T^2)^2} \left[(m_H^2 - \hat{t}) F_t(\hat{t}) \left(G_t(\hat{t}, \hat{u}) - G_b(\hat{t}, \hat{u}) \right) - (\hat{t} \leftrightarrow \hat{u}) \right], \quad (\text{A.17})$$

$$\begin{aligned} \mathcal{A}_4^{(1,\boxtimes)} &= -\frac{m_t^2}{4\sqrt{2} m_Z \hat{s}^2 (m_Z^2 + p_T^2)^2} \left[(m_Z^2 (m_H^2 - \hat{t})^2 \right. \\ &\quad \left. - \hat{t} (m_Z^2 - \hat{u})^2) F_t(\hat{t}) \left(G_t(\hat{t}, \hat{u}) - G_b(\hat{t}, \hat{u}) \right) - (\hat{t} \leftrightarrow \hat{u}) \right], \end{aligned} \quad (\text{A.18})$$

$$\begin{aligned} \mathcal{A}_5^{(1,\boxtimes)} &= -\frac{m_t^2 p_T}{4\sqrt{6} \hat{s} (m_Z^2 + p_T^2)^2} \left[(4m_Z^2 - \hat{s} - 4\hat{u}) F_t(\hat{t}) \left(G_t(\hat{t}, \hat{u}) - G_b(\hat{t}, \hat{u}) \right) \right. \\ &\quad \left. - (\hat{t} \leftrightarrow \hat{u}) \right], \end{aligned} \quad (\text{A.19})$$

$$\mathcal{A}_6^{(1,\boxtimes)} = 0, \quad (\text{A.20})$$

where

$$\begin{aligned} F_t(\hat{t}) &= \frac{1}{(m_H^2 - \hat{t})^2} \left[2\hat{t} (B_0(\hat{t}, m_t^2, m_t^2) - B_0(m_H^2, m_t^2, m_t^2)) \right. \\ &\quad \left. + (m_H^2 - \hat{t}) \left((m_H^2 - 4m_t^2 - \hat{t}) C_0(0, m_H^2, \hat{t}, m_t^2, m_t^2, m_t^2) - 2 \right) \right], \end{aligned} \quad (\text{A.21})$$

$$\begin{aligned} G_x(\hat{t}, \hat{u}) &= (m_Z^2 - \hat{u}) \left[m_Z^2 (B_0(\hat{t}, m_x^2, m_x^2) - B_0(m_Z^2, m_x^2, m_x^2)) \right. \\ &\quad \left. + (\hat{t} - m_Z^2) (2m_x^2 C_0(0, \hat{t}, m_Z^2, m_x^2, m_x^2, m_x^2) + 1) \right]. \end{aligned} \quad (\text{A.22})$$

Bibliography

- [1] R. A. Minlos, *Introduction to mathematical statistical physics*. No. 19. American Mathematical Soc., 2000.
- [2] M. Gell-Mann, “The eightfold way: A theory of strong interaction symmetry,” <https://www.osti.gov/biblio/4008239>.
- [3] C. N. Yang and R. L. Mills, “Conservation of isotopic spin and isotopic gauge invariance,” *Phys. Rev.* **96** (Oct, 1954) 191–195.
<https://link.aps.org/doi/10.1103/PhysRev.96.191>.
- [4] **Particle Data Group** Collaboration, P. Zyla *et al.*, “Review of Particle Physics,” *PTEP* **2020** no. 8, (2020) 083C01.
- [5] D. S. Freed, “Lectures on topological quantum field theory,” 1993.
- [6] R. Dijkgraaf and E. Witten, “Topological gauge theories and group cohomology,” *Communications in Mathematical Physics* **129** no. 2, (1990) 393–429.
- [7] A. Salam and J. C. Ward, “On a gauge theory of elementary interactions,” *Il Nuovo Cimento (1955-1965)* **19** no. 1, (1961) 165–170.
<https://doi.org/10.1007/BF02812723>.
- [8] A. Salam and J. C. Ward, “Weak and electromagnetic interactions,” *Il Nuovo Cimento (1955-1965)* **11** no. 4, (1959) 568–577.
<https://doi.org/10.1007/BF02726525>.
- [9] S. Weinberg, “A model of leptons,” *Phys. Rev. Lett.* **19** (Nov, 1967) 1264–1266.
<https://link.aps.org/doi/10.1103/PhysRevLett.19.1264>.
- [10] F. Capozzi, E. Lisi, A. Marrone, D. Montanino, and A. Palazzo, “Neutrino masses and mixings: Status of known and unknown 3ν parameters,” *Nucl. Phys. B* **908** (2016) 218–234, [arXiv:1601.07777](https://arxiv.org/abs/1601.07777) [hep-ph].
- [11] **ALEPH, DELPHI, L3, OPAL, SLD, LEP Electroweak Working Group, SLD Electroweak Group, SLD Heavy Flavour Group** Collaboration, S. Schael *et al.*, “Precision electroweak measurements on the Z resonance,” *Phys. Rept.* **427** (2006) 257–454, [arXiv:hep-ex/0509008](https://arxiv.org/abs/hep-ex/0509008).

- [12] **SLD** Collaboration, K. Abe *et al.*, “First direct measurement of the parity violating coupling of the Z^0 to the s quark,” *Phys. Rev. Lett.* **85** (2000) 5059–5063, [arXiv:hep-ex/0006019](#).
- [13] **CDF, D0** Collaboration, T. E. W. Group, “2012 Update of the Combination of CDF and D0 Results for the Mass of the W Boson,” [arXiv:1204.0042 \[hep-ex\]](#).
- [14] **ALEPH, DELPHI, L3, OPAL, LEP Electroweak** Collaboration, S. Schael *et al.*, “Electroweak Measurements in Electron-Positron Collisions at W -Boson-Pair Energies at LEP,” *Phys. Rept.* **532** (2013) 119–244, [arXiv:1302.3415 \[hep-ex\]](#).
- [15] **DØ** Collaboration, V. M. Abazov *et al.*, “Measurement of $\sin^2 \theta_{\text{eff}}^\ell$ and Z -light quark couplings using the forward-backward charge asymmetry in $p\bar{p} \rightarrow Z/\gamma^* \rightarrow e^+e^-$ events with $\mathcal{L} = 5.0 \text{ fb}^{-1}$ at $\sqrt{s} = 1.96 \text{ TeV}$,” *Phys. Rev. D* **84** (2011) 012007, [arXiv:1104.4590 \[hep-ex\]](#).
- [16] **CMS** Collaboration, V. Khachatryan *et al.*, “Measurement of the t -channel single-top-quark production cross section and of the $|V_{tb}|$ CKM matrix element in pp collisions at $\sqrt{s} = 8 \text{ TeV}$,” *JHEP* **06** (2014) 090, [arXiv:1403.7366 \[hep-ex\]](#).
- [17] **ATLAS** Collaboration, M. Aaboud *et al.*, “Measurement of the W -boson mass in pp collisions at $\sqrt{s} = 7 \text{ TeV}$ with the ATLAS detector,” *Eur. Phys. J. C* **78** no. 2, (2018) 110, [arXiv:1701.07240 \[hep-ex\]](#). [Erratum: *Eur. Phys. J. C* **78**, 898 (2018)].
- [18] Y. Nambu, “Quasi-particles and gauge invariance in the theory of superconductivity,” *Phys. Rev.* **117** (Feb, 1960) 648–663. <https://link.aps.org/doi/10.1103/PhysRev.117.648>.
- [19] J. Goldstone, “Field theories with superconductor solutions,” *Il Nuovo Cimento (1955-1965)* **19** no. 1, (1961) 154–164.
- [20] J. Goldstone, A. Salam, and S. Weinberg, “Broken symmetries,” *Phys. Rev.* **127** (Aug, 1962) 965–970. <https://link.aps.org/doi/10.1103/PhysRev.127.965>.
- [21] P. W. Anderson, “Plasmons, gauge invariance, and mass,” *Phys. Rev.* **130** (Apr, 1963) 439–442. <https://link.aps.org/doi/10.1103/PhysRev.130.439>.
- [22] F. Englert and R. Brout, “Broken symmetry and the mass of gauge vector mesons,” *Phys. Rev. Lett.* **13** (Aug, 1964) 321–323. <https://link.aps.org/doi/10.1103/PhysRevLett.13.321>.

-
- [23] P. W. Higgs, “Broken symmetries and the masses of gauge bosons,” *Phys. Rev. Lett.* **13** (Oct, 1964) 508–509.
<https://link.aps.org/doi/10.1103/PhysRevLett.13.508>.
- [24] G. S. Guralnik, C. R. Hagen, and T. W. B. Kibble, “Global conservation laws and massless particles,” *Phys. Rev. Lett.* **13** (Nov, 1964) 585–587.
<https://link.aps.org/doi/10.1103/PhysRevLett.13.585>.
- [25] G. S. Guralnik, “The History of the Guralnik, Hagen and Kibble development of the Theory of Spontaneous Symmetry Breaking and Gauge Particles,” *Int. J. Mod. Phys. A* **24** (2009) 2601–2627, [arXiv:0907.3466](https://arxiv.org/abs/0907.3466) [physics.hist-ph].
- [26] CMS Collaboration, S. Chatrchyan *et al.*, “Observation of a New Boson at a Mass of 125 GeV with the CMS Experiment at the LHC,” *Phys. Lett. B* **716** (2012) 30–61, [arXiv:1207.7235](https://arxiv.org/abs/1207.7235) [hep-ex].
- [27] ATLAS Collaboration, G. Aad *et al.*, “Observation of a new particle in the search for the Standard Model Higgs boson with the ATLAS detector at the LHC,” *Phys. Lett. B* **716** (2012) 1–29, [arXiv:1207.7214](https://arxiv.org/abs/1207.7214) [hep-ex].
- [28] N. Cabibbo, “Unitary symmetry and leptonic decays,” *Phys. Rev. Lett.* **10** (Jun, 1963) 531–533. <https://link.aps.org/doi/10.1103/PhysRevLett.10.531>.
- [29] M. Kobayashi and T. Maskawa, “CP-Violation in the Renormalizable Theory of Weak Interaction,” *Progress of Theoretical Physics* **49** no. 2, (02, 1973) 652–657, <https://academic.oup.com/ptp/article-pdf/49/2/652/5257692/49-2-652.pdf>.
<https://doi.org/10.1143/PTP.49.652>.
- [30] R. E. Behrends, R. J. Finkelstein, and A. Sirlin, “Radiative corrections to decay processes,” *Phys. Rev.* **101** (Jan, 1956) 866–873.
<https://link.aps.org/doi/10.1103/PhysRev.101.866>.
- [31] T. Kinoshita and A. Sirlin, “Radiative corrections to fermi interactions,” *Phys. Rev.* **113** (Mar, 1959) 1652–1660.
<https://link.aps.org/doi/10.1103/PhysRev.113.1652>.
- [32] I. Mohammad and A. Donnachie, “Radiative Corrections to Radiative Muon Decay,”.
- [33] T. van Ritbergen and R. G. Stuart, “Complete 2-loop quantum electrodynamic contributions to the muon lifetime in the fermi model,” *Phys. Rev. Lett.* **82** (Jan, 1999) 488–491. <https://link.aps.org/doi/10.1103/PhysRevLett.82.488>.
- [34] D. Ross and M. Veltman, “Neutral currents and the higgs mechanism,” *Nuclear Physics B* **95** no. 1, (1975) 135–147.
<https://www.sciencedirect.com/science/article/pii/055032137590485X>.

- [35] A. Djouadi, “The Anatomy of electro-weak symmetry breaking. I: The Higgs boson in the standard model,” *Phys. Rept.* **457** (2008) 1–216, [arXiv:hep-ph/0503172](#).
- [36] M. J. Dugan, H. Georgi, and D. B. Kaplan, “Anatomy of a composite higgs model,” *Nuclear Physics* **254** (1985) 299–326.
- [37] C. T. Hill and E. H. Simmons, “Strong Dynamics and Electroweak Symmetry Breaking,” *Phys. Rept.* **381** (2003) 235–402, [arXiv:hep-ph/0203079](#). [Erratum: *Phys.Rept.* 390, 553–554 (2004)].
- [38] M. Schwartz, *Quantum Field Theory and the Standard Model*. Quantum Field Theory and the Standard Model. Cambridge University Press, 2014. <https://books.google.nl/books?id=HbdEAgAAQBAJ>.
- [39] M. Peskin and D. Schroeder, *An Introduction To Quantum Field Theory*. Frontiers in Physics. Avalon Publishing, 1995. <https://books.google.de/books?id=EVeNNcslvX0C>.
- [40] M. Einhorn, D. Jones, and M. Veltman, “Heavy particles and the rho parameter in the standard model,” *Nuclear Physics B* **191** no. 1, (1981) 146–172. <https://www.sciencedirect.com/science/article/pii/0550321381902923>.
- [41] M. E. Peskin and T. Takeuchi, “New constraint on a strongly interacting higgs sector,” *Phys. Rev. Lett.* **65** (Aug, 1990) 964–967. <https://link.aps.org/doi/10.1103/PhysRevLett.65.964>.
- [42] M. E. Peskin and T. Takeuchi, “Estimation of oblique electroweak corrections,” 1991.
- [43] M. Golden and L. Randall, “Radiative corrections to electroweak parameters in technicolor theories,” *Nuclear Physics B* **361** no. 1, (1991) 3–23. <https://www.sciencedirect.com/science/article/pii/0550321391906144>.
- [44] B. Holdom and J. Terning, “Large corrections to electroweak parameters in technicolor theories,” *Physics Letters B* **247** no. 1, (1990) 88–92. <https://www.sciencedirect.com/science/article/pii/037026939091054F>.
- [45] G. Altarelli, R. Barbieri, and S. Jadach, “Toward a model-independent analysis of electroweak data,” *Nuclear Physics B* **369** no. 1, (1992) 3–32. <https://www.sciencedirect.com/science/article/pii/055032139290376M>.
- [46] R. S. Chivukula, S. B. Selipsky, and E. H. Simmons, “Nonoblique effects in the zbb^- vertex from extended technicolor dynamics,” *Phys. Rev. Lett.* **69** (Jul, 1992) 575–577. <https://link.aps.org/doi/10.1103/PhysRevLett.69.575>.

-
- [47] E. H. Simmons, R. S. Chivukula, and J. Terning, “Testing extended technicolor with $R(b)$,” *Prog. Theor. Phys. Suppl.* **123** (1996) 87–96, [arXiv:hep-ph/9509392](#).
 - [48] **ATLAS** Collaboration, M. Aaboud *et al.*, “Observation of $H \rightarrow b\bar{b}$ decays and VH production with the ATLAS detector,” *Phys. Lett. B* **786** (2018) 59–86, [arXiv:1808.08238 \[hep-ex\]](#).
 - [49] **CMS** Collaboration, A. M. Sirunyan *et al.*, “Observation of Higgs boson decay to bottom quarks,” *Phys. Rev. Lett.* **121** no. 12, (2018) 121801, [arXiv:1808.08242 \[hep-ex\]](#).
 - [50] T. Han and S. Willenbrock, “QCD correction to the $p p \rightarrow W H$ and $Z H$ total cross-sections,” *Phys. Lett. B* **273** (1991) 167–172.
 - [51] O. Brein, A. Djouadi, and R. Harlander, “NNLO QCD corrections to the Higgs-strahlung processes at hadron colliders,” *Phys. Lett. B* **579** (2004) 149–156, [arXiv:hep-ph/0307206](#).
 - [52] S. Amoroso *et al.*, “Les Houches 2019: Physics at TeV Colliders: Standard Model Working Group Report,” in *11th Les Houches Workshop on Physics at TeV Colliders: PhysTeV Les Houches*. 3, 2020. [arXiv:2003.01700 \[hep-ph\]](#).
 - [53] M. Cepeda *et al.*, “Report from Working Group 2: Higgs Physics at the HL-LHC and HE-LHC,” *CERN Yellow Rep. Monogr.* **7** (2019) 221–584, [arXiv:1902.00134 \[hep-ph\]](#).
 - [54] C. Englert, M. McCullough, and M. Spannowsky, “Gluon-initiated associated production boosts Higgs physics,” *Phys. Rev. D* **89** no. 1, (2014) 013013, [arXiv:1310.4828 \[hep-ph\]](#).
 - [55] C. Englert, R. Rosenfeld, M. Spannowsky, and A. Tonero, “New physics and signal-background interference in associated $pp \rightarrow HZ$ production,” *EPL* **114** no. 3, (2016) 31001, [arXiv:1603.05304 \[hep-ph\]](#).
 - [56] R. V. Harlander, S. Liebler, and T. Zirke, “Higgs Strahlung at the Large Hadron Collider in the 2-Higgs-Doublet Model,” *JHEP* **02** (2014) 023, [arXiv:1307.8122 \[hep-ph\]](#).
 - [57] B. A. Kniehl, “Associated Production of Higgs and Z Bosons From Gluon Fusion in Hadron Collisions,” *Phys. Rev. D* **42** (1990) 2253–2258.
 - [58] D. A. Dicus and C. Kao, “Higgs Boson - Z^0 Production From Gluon Fusion,” *Phys. Rev. D* **38** (1988) 1008. [Erratum: *Phys.Rev.D* 42, 2412 (1990)].

- [59] L. Altenkamp, S. Dittmaier, R. V. Harlander, H. Rzehak, and T. J. Zirke, “Gluon-induced Higgs-strahlung at next-to-leading order QCD,” *JHEP* **02** (2013) 078, [arXiv:1211.5015 \[hep-ph\]](#).
- [60] R. V. Harlander, A. Kulesza, V. Theeuwes, and T. Zirke, “Soft gluon resummation for gluon-induced Higgs Strahlung,” *JHEP* **11** (2014) 082, [arXiv:1410.0217 \[hep-ph\]](#).
- [61] A. Hasselhuhn, T. Luthe, and M. Steinhauser, “On top quark mass effects to $gg \rightarrow ZH$ at NLO,” *JHEP* **01** (2017) 073, [arXiv:1611.05881 \[hep-ph\]](#).
- [62] R. Harlander, J. Klappert, C. Pandini, and A. Papaefstathiou, “Exploiting the WH/ZH symmetry in the search for New Physics,” *Eur. Phys. J. C* **78** no. 9, (2018) 760, [arXiv:1804.02299 \[hep-ph\]](#).
- [63] B. Hespel, F. Maltoni, and E. Vryonidou, “Higgs and Z boson associated production via gluon fusion in the SM and the 2HDM,” *JHEP* **06** (2015) 065, [arXiv:1503.01656 \[hep-ph\]](#).
- [64] J. Davies, G. Mishima, and M. Steinhauser, “Virtual corrections to $gg \rightarrow ZH$ in the high-energy and large- m_t limits,” [arXiv:2011.12314 \[hep-ph\]](#).
- [65] L. Chen, G. Heinrich, S. P. Jones, M. Kerner, J. Klappert, and J. Schlenk, “ZH production in gluon fusion: two-loop amplitudes with full top quark mass dependence,” [arXiv:2011.12325 \[hep-ph\]](#).
- [66] R. Bonciani, G. Degrandi, P. P. Giardino, and R. Gröber, “Analytical Method for Next-to-Leading-Order QCD Corrections to Double-Higgs Production,” *Phys. Rev. Lett.* **121** no. 16, (2018) 162003, [arXiv:1806.11564 \[hep-ph\]](#).
- [67] L. D. Landau, “On the angular momentum of a system of two photons,” *Dokl. Akad. Nauk SSSR* **60** no. 2, (1948) 207–209.
- [68] C.-N. Yang, “Selection Rules for the Dematerialization of a Particle Into Two Photons,” *Phys. Rev.* **77** (1950) 242–245.
- [69] M. Spira, A. Djouadi, D. Graudenz, and P. M. Zerwas, “Higgs boson production at the LHC,” *Nucl. Phys. B* **453** (1995) 17–82, [arXiv:hep-ph/9504378](#).
- [70] U. Aglietti, R. Bonciani, G. Degrandi, and A. Vicini, “Analytic Results for Virtual QCD Corrections to Higgs Production and Decay,” *JHEP* **01** (2007) 021, [arXiv:hep-ph/0611266](#).
- [71] G. Degrandi and P. Slavich, “NLO QCD bottom corrections to Higgs boson production in the MSSM,” *JHEP* **11** (2010) 044, [arXiv:1007.3465 \[hep-ph\]](#).

-
- [72] G. Passarino and M. J. G. Veltman, “One Loop corrections for e^+e^- annihilation into $\mu^+\mu^-$ in the Weinberg Model,” *Nucl. Phys.* **B160** (1979) 151.
 - [73] T. Hahn, “Generating Feynman diagrams and amplitudes with FeynArts 3,” *Comput. Phys. Commun.* **140** (2001) 418–431, [arXiv:hep-ph/0012260](#).
 - [74] R. Mertig, M. Bohm, and A. Denner, “FEYN CALC: Computer algebraic calculation of Feynman amplitudes,” *Comput. Phys. Commun.* **64** (1991) 345–359.
 - [75] V. Shtabovenko, R. Mertig, and F. Orellana, “New Developments in FeynCalc 9.0,” *Comput. Phys. Commun.* **207** (2016) 432–444, [arXiv:1601.01167 \[hep-ph\]](#).
 - [76] S. Larin, “The Renormalization of the axial anomaly in dimensional regularization,” *Phys. Lett. B* **303** (1993) 113–118, [arXiv:hep-ph/9302240](#).
 - [77] G. Degrandi, S. Di Vita, and P. Slavich, “NLO QCD corrections to pseudoscalar Higgs production in the MSSM,” *JHEP* **08** (2011) 128, [arXiv:1107.0914 \[hep-ph\]](#).
 - [78] L. F. Abbott, “The Background Field Method Beyond One Loop,” *Nucl. Phys. B* **185** (1981) 189–203.
 - [79] A. V. Smirnov, “FIRE5: a C++ implementation of Feynman Integral REduction,” *Comput. Phys. Commun.* **189** (2015) 182–191, [arXiv:1408.2372 \[hep-ph\]](#).
 - [80] R. N. Lee, “LiteRed 1.4: a powerful tool for reduction of multiloop integrals,” *J. Phys. Conf. Ser.* **523** (2014) 012059, [arXiv:1310.1145 \[hep-ph\]](#).
 - [81] A. von Manteuffel and L. Tancredi, “A non-planar two-loop three-point function beyond multiple polylogarithms,” *JHEP* **06** (2017) 127, [arXiv:1701.05905 \[hep-ph\]](#).
 - [82] R. Bonciani, G. Degrandi, P. P. Giardino, and R. Gröber, “A Numerical Routine for the Crossed Vertex Diagram with a Massive-Particle Loop,” *Comput. Phys. Commun.* **241** (2019) 122–131, [arXiv:1812.02698 \[hep-ph\]](#).
 - [83] G. Degrandi, P. P. Giardino, and R. Gröber, “On the two-loop virtual QCD corrections to Higgs boson pair production in the Standard Model,” *Eur. Phys. J. C* **76** no. 7, (2016) 411, [arXiv:1603.00385 \[hep-ph\]](#).
 - [84] O. Eboli, G. Marques, S. Novaes, and A. Natale, “Twin higgs-boson production,” *Physics Letters B* **197** no. 1, (1987) 269 – 272.

- [85] E. Glover and J. van der Bij, “Higgs boson pair production via gluon fusion,” *Nuclear Physics B* **309** no. 2, (1988) 282 – 294.
- [86] D. A. Dicus, C. Kao, and S. S. D. Willenbrock, “Higgs Boson Pair Production From Gluon Fusion,” *Phys. Lett.* **B203** (1988) 457–461.
- [87] T. Plehn, M. Spira, and P. M. Zerwas, “Pair production of neutral Higgs particles in gluon-gluon collisions,” *Nucl. Phys.* **B479** (1996) 46–64, [arXiv:hep-ph/9603205 \[hep-ph\]](#). [Erratum: Nucl. Phys.B531,655(1998)].
- [88] S. Dawson, S. Dittmaier, and M. Spira, “Neutral Higgs boson pair production at hadron colliders: QCD corrections,” *Phys. Rev.* **D58** (1998) 115012, [arXiv:hep-ph/9805244 \[hep-ph\]](#).
- [89] S. Borowka, N. Greiner, G. Heinrich, S. P. Jones, M. Kerner, J. Schlenk, and T. Zirke, “Full top quark mass dependence in Higgs boson pair production at NLO,” *JHEP* **10** (2016) 107, [arXiv:1608.04798 \[hep-ph\]](#).
- [90] S. Borowka, N. Greiner, G. Heinrich, S. P. Jones, M. Kerner, J. Schlenk, U. Schubert, and T. Zirke, “Higgs Boson Pair Production in Gluon Fusion at Next-to-Leading Order with Full Top-Quark Mass Dependence,” *Phys. Rev. Lett.* **117** no. 1, (2016) 012001, [arXiv:1604.06447 \[hep-ph\]](#). [Erratum: Phys. Rev. Lett.117,no.7,079901(2016)].
- [91] J. Baglio, F. Campanario, S. Glaus, M. Mühlleitner, M. Spira, and J. Streicher, “Gluon fusion into Higgs pairs at NLO QCD and the top mass scheme,” *Eur. Phys. J.* **C79** no. 6, (2019) 459, [arXiv:1811.05692 \[hep-ph\]](#).
- [92] G. Heinrich, S. P. Jones, M. Kerner, G. Luisoni, and L. Scyboz, “Probing the trilinear Higgs boson coupling in di-Higgs production at NLO QCD including parton shower effects,” *JHEP* **06** (2019) 066, [arXiv:1903.08137 \[hep-ph\]](#).
- [93] J. Davies, R. Gröber, A. Maier, T. Rauh, and M. Steinhauser, “Top quark mass dependence of the Higgs boson-gluon form factor at three loops,” *Phys. Rev.* **D100** no. 3, (2019) 034017, [arXiv:1906.00982 \[hep-ph\]](#).
- [94] M. Grazzini, G. Heinrich, S. Jones, S. Kallweit, M. Kerner, J. M. Lindert, and J. Mazzitelli, “Higgs boson pair production at NNLO with top quark mass effects,” *JHEP* **05** (2018) 059, [arXiv:1803.02463 \[hep-ph\]](#).
- [95] **NNPDF** Collaboration, R. D. Ball *et al.*, “Parton distributions from high-precision collider data,” *Eur. Phys. J.* **C77** no. 10, (2017) 663, [arXiv:1706.00428 \[hep-ph\]](#).

- [96] A. Buckley, J. Ferrando, S. Lloyd, K. Nordström, B. Page, M. Rüfenacht, M. Schönherr, and G. Watt, “LHAPDF6: parton density access in the LHC precision era,” *Eur. Phys. J. C* **75** (2015) 132, [arXiv:1412.7420 \[hep-ph\]](#).
- [97] A. Denner, S. Dittmaier, and L. Hofer, “COLLIER - A fortran-library for one-loop integrals,” *PoS LL2014* (2014) 071, [arXiv:1407.0087 \[hep-ph\]](#).
- [98] S. Dittmaier *et al.*, “Handbook of LHC Higgs Cross Sections: 2. Differential Distributions,” [arXiv:1201.3084 \[hep-ph\]](#).
- [99] **LHC Higgs Cross Section Working Group** Collaboration, D. de Florian *et al.*, “Handbook of LHC Higgs Cross Sections: 4. Deciphering the Nature of the Higgs Sector,” [arXiv:1610.07922 \[hep-ph\]](#).
- [100] A. D. Martin, W. J. Stirling, R. S. Thorne, and G. Watt, “Uncertainties on $\alpha(S)$ in global PDF analyses and implications for predicted hadronic cross sections,” *Eur. Phys. J. C* **64** (2009) 653–680, [arXiv:0905.3531 \[hep-ph\]](#).
- [101] F. Demartin, S. Forte, E. Mariani, J. Rojo, and A. Vicini, “The impact of PDF and alphas uncertainties on Higgs Production in gluon fusion at hadron colliders,” *Phys. Rev. D* **82** (2010) 014002, [arXiv:1004.0962 \[hep-ph\]](#).
- [102] J. Baglio, A. Djouadi, R. Gröber, M. M. Mühlleitner, J. Quevillon, and M. Spira, “The measurement of the Higgs self-coupling at the LHC: theoretical status,” *JHEP* **04** (2013) 151, [arXiv:1212.5581 \[hep-ph\]](#).

List of publications

1. **L. Alasfar**, G. Degrassi, P. P. Giardino, R. Gröber and M. Vitti
Virtual corrections to $gg \rightarrow ZH$ via a transverse momentum expansion
JHEP **05** (2021), 168
arXiv:2103.06225 [hep-ph].
2. **L. Alasfar**, A. Azatov, J. de Blas, A. Paul and M. Valli
 B anomalies under the lens of electroweak precision
JHEP **12** (2020), 016
arXiv:2007.04400 [hep-ph].
3. **L. Alasfar**, R. Corral Lopez and R. Gröber
Probing Higgs couplings to light quarks via Higgs pair production
JHEP **11** (2019), 088
arXiv:1909.05279 [hep-ph].